Available online at www.sciencedirect.com

ScienceDirect

Geochimica et Cosmochimica Acta 307 (2021) 281–301

Geochimica et Cosmochimica Acta

www.elsevier.com/locate/gca

Chronological constraints on the thermal evolution of ordinary chondrite parent bodies from the ^{53}Mn-^{53}Cr system

Aryavart Anand [a,*], Jonas Pape [a,b], Martin Wille [a], Klaus Mezger [a]

[a] *Institut für Geologie, Universität Bern, Baltzerstrasse 1+3, 3012 Bern, Switzerland*
[b] *Institut für Planetologie, Universität Münster, Wilhelm-Klemm-Str. 10, 48149 Münster, Germany*

Received 25 November 2020; accepted in revised form 23 April 2021; Available online 1 May 2021

Abstract

The ^{53}Mn-^{53}Cr isotope systematics in ordinary chondrites constrains the accretion and thermal history of their parent bodies. Mineralogical observations and olivine-spinel geothermometry suggest that chromite in ordinary chondrites formed during prograde thermal metamorphism with the amount of chromite increasing with petrologic grades in type 3 to type 6 ordinary chondrites. Assuming a chondritic evolution of the respective parent bodies, ^{53}Cr/^{52}Cr model ages for chromite range from $3.99^{+0.93}_{-0.79}$ to $11.1^{+6.0}_{-2.8}$ Ma after the formation of calcium-aluminium-rich inclusions (CAIs). Chromite and silicate-metal-sulphide isochrons define an age range from $2.78^{+0.55}_{-0.50}$ to $15.4^{+2.4}_{-1.6}$ Ma. Both chromite model ages and isochron ages correlate with the petrological grade of the samples, which is consistent with an onion-shell structure of the chondrite parent bodies. The study shows that unlike the isochron ages, which are prone to impact-related disturbances or partial re-equilibration during cooling from high temperatures, the chromite model ages are not easily affected by thermal metamorphism or later events and yield robust mineral growth ages. The results are consistent with a homogenous distribution of ^{53}Mn and an initial canonical $^{53}Mn/^{55}Mn = 6.28 \times 10^{-6}$. The estimated closure temperatures for the Mn-Cr system in chromites range from ~760 °C for type 6 to ~540–620 °C for type 3 ordinary chondrites. The high closure temperatures estimated for type 3 and type 6 ordinary chondrites imply that the chromite ages correspond to the peak metamorphic temperature reached during the thermal history of the chondrite parent bodies. The oldest chromite model age obtained for type 3 samples along with the established Al-Mg chondrule formation ages constrain the accretion of the parent bodies to >2.1 Ma after CAI formation, implying that planetesimal accretion immediately followed chondrule formation.

Keywords: Ordinary Chondrites; Olivine-Spinel Geothermometry; Cr isotopes; Closure Temperature; Thermal Evolution; Accretion

1. INTRODUCTION

Ordinary chondrites are among the solar system's most primitive materials, containing early formed solids, including chondrules, calcium-aluminium rich inclusions (CAIs), metallic Fe-Ni grains and fine-grained matrix. The ordinary chondrite clan is subdivided into H, L and LL groups based on distinct metal to silicate ratios and each of these groups is thought to sample a distinct parent body in the Main Asteroid Belt. The ordinary chondrites were metamorphosed to different degrees, but never experienced global melting and differentiation. They are divided into petrological types ranging from petrological type 3 (unequilibrated, low thermal overprint) to types 4–6 (equilibrated, higher metamorphic grades) (Van Schmus and Wood, 1967). The degree of chemical homogeneity of various phases in relationship to the petrologic type and response to the onset and progressive thermal metamorphism has been an

* Corresponding author.
E-mail addresses: aryavart.anand@geo.unibe.ch (A. Anand), jonas.pape@uni-muenster.de (J. Pape), martin.wille@geo.unibe.ch (M. Wille), klaus.mezger@geo.unibe.ch (K. Mezger).

https://doi.org/10.1016/j.gca.2021.04.029
0016-7037/

important issue in numerous studies of ordinary chondrites (e.g., Grossman and Brearley, 2005; Kimura et al., 2006; Kessel et al., 2007). The onset of metamorphism is manifested in the formation of new phases and the homogenisation in and among minerals in a given sample. Critical time information about the accretion and metamorphism of the parent bodies of ordinary chondrites can be acquired from chronological studies using short-lived radionuclides (e.g., ^{182}Hf, ^{53}Mn, ^{26}Al) with half-lives of 10^5–10^8 years.

Grossman and Brearley (2005) showed that the onset of metamorphism in ordinary chondrites leads to the exsolution of Cr from olivine as fine-grained opaque phases, probably in the form of chromite ($FeCr_2O_4$). Kimura et al. (2006) reported an increase in the abundance and compositional changes of spinel group minerals that can be explained with progressive thermal metamorphism. Chromite, together with olivine has also been used in olivine-spinel thermometry and shows a systematic increase in the maximum temperature correlating with the metamorphic type, recorded by individual chondrites (Wlotzka, 2005; Kessel et al., 2007).

The formation of chromite can potentially be dated with the ^{53}Mn-^{53}Cr system thus providing time constraints on new mineral growth on the parent body. The short-lived radionuclide ^{53}Mn ($t_{1/2}$ = 3.7 ± 0.4 Ma, Honda and Imamura, 1971) has long been recognized (Birck and Allègre, 1985a) and used for high-resolution chronological studies of chondrites to date processes and events within the first ~20 Ma of solar system history (Lugmair and Shukolyukov, 1998; Nyquist et al., 2001; Shukolyukov and Lugmair, 2006; Trinquier et al., 2008a, b; Göpel et al., 2015). One of the advantages of using the Mn-Cr chronometer is that Mn and Cr are abundant elements in ordinary chondrites and their components have variable and/or high Mn/Cr ratios, which makes them suitable for dating by constructing an isochron. Alternatively, the Cr-isotopes can be used to obtain precise "model ages" for minerals with a Mn/Cr ratio near zero, which is the case for chromite, a mineral that occurs in meteorites of all ordinary chondrite groups. Chromite preserves initial ^{53}Cr/^{52}Cr ratios corresponding to the time of isotope closure of the Mn-Cr system and this isotope ratio can be measured with high precision. A model age can be obtained by comparing the Cr-isotopic composition of the chromite with the Cr-isotope evolution of its assumed reservoir. The Mn-Cr chromite model ages for ordinary chondrites along with the closure temperature estimate of Cr in spinel open up the possibility of using the Mn-Cr system to construct well constrained thermal evolution models or evaluating the validity of existing ones.

In addition to the derivation of model ages, chromites in combination with silicates in single meteorite samples can also be used to construct isochrons. The combination of the two types of age estimates provides temporal constraints on the thermal evolution of meteorite parent bodies, sets time limits for the interval of their accretion and their cooling history, which are a function of accretion time and size of the bodies.

This study reports chromite model ages along with two-point isochron ages from a group of type 3 (unequilibrated) and type 6 (equilibrated) samples. The age data along with petrographical and olivine-spinel geothermometry provides new constraints on the accretion time and metamorphic history of the ordinary chondrite parent bodies.

2. SAMPLES AND ANALYTICAL METHODS

A total of 8 samples of H and L ordinary chondrites were selected for ^{53}Mn-^{53}Cr dating. The samples are from the Omani-Swiss meteorite search collection stored at the Natural History Museum Bern. Four of these samples are of low petrologic grade (type 3) and include Sayh al Uhaymir 246 (SaU 246, H3/4), Ramlat as Sahmah 337 (RaS 337, H3.6), Jiddat al Harasis 596 (JaH 596, L3) and Ramlat as Sahmah 265 (RaS 265, L3). The other four chondrites are of petrologic type 6 and include Jiddat al Harasis 578 (JaH 578, H6), Sayh al Uhaymir 228 (SaU 228, H6), Dhofar 1012 (Dho 1012, L6) and Al Huwaysah 017 (no official abbreviation, henceforth AHu 017, L6). Most samples record low shock (S1-2) except Dho 1012 (S3) and AHu 017 (S4). The samples SaU 246, RaS 337 and JaH 596 are classified as W3 on the W0-W6 weathering classification of Wlotzka (1993), while all the other samples are classified as W1 or W2.

Petrographical studies were performed with an Olympus BX51 microscope equipped with a digital camera using plane and cross-polarized light. Thin section mosaics were created with an MIA (multiple imaging analyzer) stage attached to the microscope and used as a reference during subsequent scanning electron microscope (SEM) and electron microprobe investigations at the Institute of Geological Sciences, University of Bern.

Backscattered electron (BSE) imaging and mineral identification via energy-dispersive X-ray spectroscopy (EDS) were conducted on a ZEISS EVO50 SEM. Spinel (sensu lato) grains were identified in all the samples and their textural response to metamorphism in relationship to the petrologic type was evaluated. Olivine-spinel pairs in the chondrules of type 3 and chondrules and matrices of type 6 chondrites were selected for Fe-Mg exchange geothermometry. Only those pairs were selected where olivine and spinel are in direct contact, following the approach described in Kessel et al. (2007).

The major and minor element abundances in olivine and spinel were measured with a JEOL JXA-8200 Superprobe. Analyses were conducted as individual point measurements with the beam focused to 1 μm, the acceleration voltage set at 15 kV (all measurements) and a beam current between 15 and 20 nA. Elemental concentrations were measured using five wavelength-dispersive spectrometers (WDS) and calibrated using a set of synthetic and natural reference materials. The detection limits for all elements were typically below 100 μg/g. Automated matrix correction was done with the built-in CITZAF package (Armstrong, 1995).

For each sample, 1–1.5 g of whole-rock meteorite was hand crushed using a pre-cleaned agate mortar and transferred into a separate 15 ml Savillex® beaker. The material was partially dissolved in conc. aqua regia on a hot plate set to 90 °C for 48 hrs. The dissolved metal-sulfide fraction was transferred into a separate 60 ml Savillex® beaker. The

remaining undissolved solid was rinsed with high-purity (18.2 MΩ) MilliQ® water twice and the supernatant was added to the metal-sulfide fraction. To dissolve the silicate fraction, 4 ml of a 3:1 mixture of conc. HF and HNO_3 were added and heated up to 90 °C for 48 hrs. After cooling, the sample was dried, 4 ml 6.4 M HCl was added and put on a hot plate at 140 °C for 24 hrs to break down fluorides. Afterwards, the dissolved silicate fraction was recombined with the metal-sulfide fraction. From visual inspection, two undissolved residual phases could be identified in the beaker: chromite (spinel) and organic matter. The residual chromite grains together with the undissolved organic matter were transferred into a 15 ml centrifuge vial, gravitationally separated from each other, and siphoned into a separate beaker. The complete sample digestion process resulted in three distinct sample splits: (1) residual material consisting of pure chromite (2) dissolved material that is mostly derived from silicates, metal, and sulfides and (3) organic residue. The refractory chromite grains were hand-picked into 200 µL Savillex® vials and digested in PTFE-lined stainless-steel pressure bombs (Parr® bombs) with 10 ml conc. inverse aqua regia and placed in an oven for 96 hrs. at 190 °C. With this procedure, the chromite could be brought into solution. Hereafter, both chromite and silicate-metal-sulfide fractions were analyzed separately. The term 'silicate' is used to refer to the silicate-metal-sulfide fraction. All beakers, jars and centrifuge tubes used in the sample processing were pre-cleaned and all acids were cleaned by sub-boiling distillation.

The dissolved chromite and silicate fractions from each sample were divided into two aliquots. The first aliquot was used for the determination of Mn/Cr ratios. The second aliquot was used for chemical separation of Cr and measurement of Cr isotopes on Triton™ Plus thermal ionization mass spectrometer (TIMS) in the isotope laboratory at the University of Bern. Whenever possible, Cr isotopes of a sample were measured multiple times to obtain higher precision. The long term (9 months) reproducibility (2SD) for $\varepsilon^{53}Cr$ and $\varepsilon^{54}Cr$ including the temporal drift was 0.07 and 0.28 respectively ($n = 53$). The details of Mn/Cr ratio determination, chemical separation of Cr and TIMS measurement protocol are provided in the Supplementary Material.

2.1. Model for $\varepsilon^{53}Cr$ evolution in chondrites

The model for $\varepsilon^{53}Cr$ evolution in chondrites assumes that they represent an isotopically homogeneous reservoir in Cr and Mn space that evolved with a distinct Mn/Cr ratio after primordial nebular Mn/Cr fractionation and isolation of the precursor material of chondrites, terrestrial planets and differentiated planetesimals (Trinquier et al., 2008b). The evolution of the $^{53}Cr/^{52}Cr$ isotopic composition of the chondrite reservoir through time can be expressed as:

$$\left(^{53}Cr/^{52}Cr\right)_p = \left(^{53}Cr/^{52}Cr\right)_i + (k)\left(^{53}Mn/^{55}Mn\right)_i \times \left(1 - e^{-\lambda t}\right) \quad (1)$$

where p refers to the present values, i refers to the initial values and λ denotes the ^{53}Mn decay constant. The $^{55}Mn/^{52}Cr$ of the reservoir is denoted by k; and t represents the time elapsed since the start of the solar system, which is equated with the time of CAI formation. Eq. (1) describes the evolution of $^{53}Cr/^{52}Cr$ with time for the chondritic reservoir with a pre-determined Mn/Cr ratio and can be used to derive a model age for a chondrite sample by measuring the Cr isotopic composition of its chromite fraction only. Due to its very low Mn/Cr ratio, chromite preserves the Cr isotopic composition of its growth environment because the in-growth of radiogenic ^{53}Cr in chromite from in-situ decay of ^{53}Mn is negligible. For instance, a Mn/Cr ratio of 0.01 in typical chromite would result in an in-situ radiogenic $\varepsilon^{53}Cr$ contribution of 0.006 within 10 Myr after CAI formation, which is insignificant, compared to the $\varepsilon^{53}Cr$ evolution of 0.33 in the chondritic reservoir during this period.

Using the Cr isotopic composition of chromites to obtain model ages of their formation relies on the following assumptions: (i) homogenous distribution of ^{53}Mn in the solar system, (ii) known abundance of ^{53}Mn and ^{53}Cr at the beginning of the solar system or any point in time thereafter, and (iii) an estimate for the Mn/Cr in the relevant reservoir.

It can be assumed that the solar system had a homogeneous distribution of ^{53}Cr and ^{53}Mn at or shortly after its formation. This is evident from the identical ages of meteorites or their components derived from the Mn-Cr system and other short-lived isotope systems (e.g., Hf-W) as shown in several studies (Trinquier et al., 2008b; Nyquist et al., 2009; Kleine et al., 2012). These comparisons also give confidence in the definitions of $(^{53}Mn/^{55}Mn)_i$ and $\varepsilon^{53}Cr_i$ (Göpel et al., 2015).

The abundances of ^{53}Mn and $^{53}Cr/^{52}Cr$ at the beginning of the solar system has been determined in several studies with distinct approaches:

(i) Shukolyukov and Lugmair (2006), Moynier et al. (2007) and Göpel et al. (2015) determined the $^{53}Mn/^{55}Mn_i$ and $\varepsilon^{53}Cr_i$ by evaluating the Mn/Cr data for bulk rock carbonaceous chondrites (CC) on a $^{55}Mn/^{52}Cr$ versus $\varepsilon^{53}Cr$ diagram. Shukolyukov and Lugmair (2006) reported that the correlation line yields a $^{53}Mn/^{55}Mn$ of $8.5 \pm 1.5 \times 10^{-6}$ and initial $\varepsilon^{53}Cr = -0.21 \pm 0.09$ at the time of Mn/Cr fractionation. Göpel et al. (2015) obtained a canonical $^{53}Mn/^{55}Mn_i = 6.8 \times 10^{-6}$ and $\varepsilon^{53}Cr_i$ corresponding to −0.177 from the bulk rock CC isochron with respect to the age of the solar system. It should be noted that the whole rock CC isochrons depend strongly on the choice of which samples to include in or exclude from the linear regression (Qin et al., 2010).

(ii) Trinquier et al. (2008b) constrained $^{53}Mn/^{55}Mn_i = 6.28 \pm 0.66 \times 10^{-6}$ using an isochron based on ^{54}Cr-poor fractions of CI Orgueil and reported it as the best estimate for the initial solar system ^{53}Mn abundance. The authors back-calculated $\varepsilon^{53}Cr_i$ for a wide range of chondritic reservoirs using present-day $^{53}Cr/^{52}Cr$ and Mn/Cr ratios to the time of CAI formation and reported the average of all $\varepsilon^{53}Cr_i$ as solar system initial $\varepsilon^{53}Cr_i$ = -0.23 ± 0.09.

They additionally determined $^{53}Mn/^{55}Mn_i = 6.38 \pm 1.2 \times 10^{-6}$ at the time of CAI formation by anchoring the $^{53}Mn/^{55}Mn$ value obtained for H4 chondrite Ste. Marguerite with its predetermined ^{207}Pb-^{206}Pb phosphates age of 4562.7 ± 0.6 Ma (Göpel et al., 1994). However, Blackburn et al. (2017) reported an updated U-corrected ^{207}Pb-^{206}Pb phosphate age (=4561.7 Ma after CAIs) for Ste. Marguerite with which the $^{53}Mn/^{55}Mn_i$ derived using Ste. Marguerite systematics can be recalculated as 7.68×10^{-6}, at the time of CAI formation (4567.18 ± 0.50 Ma, Amelin et al., 2010).

For the model ages, it is assumed that the Cr isotopic evolution of the reservoir from which the chromites formed was governed by a Mn/Cr elemental ratio identical to CI chondrites (Birck et al., 1999). This approach is supported by the observation that all chondrites (except enstatites chondrites) plot on a single Mn-Cr isotopic evolution line within error starting from CI and with Mn/Cr indistinguishable from the CI reservoir (Birck et al., 1999). Bulk analyses of ordinary chondrites also indicate that their Mn/Cr is similar to the ratio in CI chondrites (Wasson and Allemeyn, 1988, Trinquier et al., 2008b; Qin et al., 2010; Pedersen et al., 2019). Moreover, bulk analyses of single chondrules from ordinary chondrites also show close to chondritic Mn/Cr ratios (e.g. Mahan et al., 2018). Hence, the Mn/Cr ratio of the CI chondrites can be used as a representative for the Mn/Cr value of the chondritic reservoir in the $\varepsilon^{53}Cr$ chondritic evolution model.

3. RESULTS

3.1. Mineral compositions

Average compositions, end-member mole percentage and corresponding standard deviations measured for olivine and spinel pairs in each sample are given in Tables 1 and 2. End member mole % for spinel (Table 2) were calculated using End Member Generator (EMG) (Ferracutti et al., 2015).

Olivine in all the samples is Mg-rich with Fayalite (Fa) ranging from 18.1 to 24.8 mole %. Olivine crystals in type 6 chondrites are equilibrated as indicated by smaller standard deviations in Fa mole % as compared to type 3 samples, RaS 265 (L3) and JaH 596 (L3), that show unequilibrated olivine compositions with larger standard deviations (Table 1). However, type 3 samples of higher petrologic subtype, SaU 246 (H3/4) and RaS 337 (H3.6), also have small standard deviations in Fa mole % similar to those of type 6 samples (see Table 1). Overall, the olivine compositions determined in this study agree with the sample classification (Table 1).

The average chromite ($FeCr_2O_4$) component of spinel in all samples is 71.5 mole %. Type 3 samples show much higher standard deviations in chromite mole % compared to type 6 samples (Table 2), which agrees with the previously reported spinel data for unequilibrated and equilibrated chondrites (Bunch et al., 1967; Keil et al., 1978a,b; Johnson and Prinz, 1991; Yanai and Kojima, 1991; Ruzicka et al., 1998).

3.2. Olivine-spinel thermometry

The olivine-spinel thermometer provides a semi-quantitative tool to relate thermal metamorphic conditions to primary indicators of the petrologic types (i.e. texture and phase homogeneity) (Kessel et al., 2007). Olivine-spinel temperatures were determined using an online version of the olivine-spinel thermometer (http://melts.ofm-research.org/CORBA_CTserver/Olv_Spn_Opx/index.php) based on thermodynamic models developed in Sack and Ghiorso (1989, 1991a,b) assuming a pressure of 1 bar. The uncertainty associated with the model is approximately ± 50 °C (1σ) (e.g., Benedix et al., 2005) which is much larger than any contribution due to analytical uncertainties and is considered as uncertainty on individual temperatures. Table 3 reports the average temperature and range of temperatures derived from all

Table 1
Olivine compositions (wt%) determined by EPMA and end member classification.

Sample	SaU 228	JaH 578	Dho 1012	AHu 017	SaU 246	RaS 337	RaS 265	JaH 596
Class/Type	H6	H6	L6	L6	H3/4	H3.6	L3	L3
#[a]	13	27	22	9	5	25	29	90
Al_2O_3	0.01 ± 0.02[b]	0.02 ± 0.04	0.02 ± 0.06	0.01 ± 0.03	0.03 ± 0.06	0.02 ± 0.02	0.03 ± 0.06	0.04 ± 0.14
CaO	0.02 ± 0.03	0.03 ± 0.03	0.02 ± 0.04	0.02 ± 0.02	0.07 ± 0.09	0.03 ± 0.03	0.06 ± 0.07	0.10 ± 0.18
FeO	17.20 ± 0.80	18.4 ± 1.2	22.9 ± 1.5	21.1 ± 2.6	17.9 ± 1.3	17.30 ± 0.98	23.1 ± 4.4	20.4 ± 11.5
SiO_2	40.25 ± 0.46	39.55 ± 0.74	38.4 ± 1.2	39.61 ± 0.44	39.94 ± 0.75	39.81 ± 0.88	38.29 ± 0.94	38.6 ± 2.2
MgO	43.37 ± 0.66	42.0 ± 1.1	38.6 ± 1.4	39.8 ± 1.9	42.33 ± 0.79	42.77 ± 0.89	39.0 ± 3.9	41.0 ± 9.2
MnO	0.49 ± 0.03	0.50 ± 0.03	0.49 ± 0.03	0.48 ± 0.04	0.47 ± 0.06	0.47 ± 0.07	0.46 ± 0.09	0.41 ± 0.21
Cr_2O_3	0.18 ± 0.32	0.08 ± 0.23	0.21 ± 0.49	0.17 ± 0.27	0.12 ± 0.05	0.03 ± 0.04	0.06 ± 0.13	0.15 ± 0.40
TiO_2	0.01 ± 0.02	0.01 ± 0.04	0.01 ± 0.03	0.02 ± 0.02	0.03 ± 0.02	0.03 ± 0.07	0.03 ± 0.08	0.01 ± 0.04
Total	101.53	100.6	100.62	101.22	100.89	100.46	100.99	100.84
Fa[c]	18.1 ± 0.9	19.6 ± 1.4	24.8 ± 1.8	22.9 ± 2.9	19.0 ± 1.4	18.4 ± 1.1	24.8 ± 5.4	21.9 ± 13.2
Lit Fa[d]	18.7	19.6	24.8	22.9	18.2–23.2	18.1 ± 0.5	11.9–26.3	25.7 ± 6.7

[a] Refers to the total number of olivine grains analyzed in each sample.
[b] 2SD of the distribution of average grain composition.
[c] Mole % of fayalite (Fa).
[d] Source: Meteoritical Bulletin Database (https://www.lpi.usra.edu/meteor/metbull.php).

Table 2
Spinel composition (wt%) determined by EPMA and end member classification.

Sample	SaU 228	JaH 578	Dho 1012	AHu 017	SaU 246	RaS 337	RaS 265	JaH 596
Class/Type	H6	H6	L6	L6	H3/4	H3.6	L3	L3
#[a]	31	26	22	22	19	6	35	17
Al_2O_3	5.89 ± 0.51[b]	5.43 ± 0.34	5.70 ± 0.53	4.66 ± 0.38	6.2 ± 3.2	4.4 ± 1.6	4.7 ± 3.6	7.7 ± 10.3
CaO	0.01 ± 0.01	0.01 ± 0.01	0.02 ± 0.05	0.03 ± 0.03	0.12 ± 0.21	0.10 ± 0.24	0.04 ± 0.05	0.06 ± 0.08
FeO[c]	28.96 ± 0.41	27.6 ± 2.0	31.0 ± 1.6	30.8 ± 1.5	28.4 ± 2.3	28.5 ± 1.2	31.0 ± 2.0	29.8 ± 2.4
MgO	3.18 ± 0.31	4.64 ± 0.65	2.44 ± 0.45	2.43 ± 0.51	2.9 ± 1.8	2.63 ± 0.55	2.2 ± 1.7	3.0 ± 1.7
MnO	1.22 ± 0.23	1.18 ± 0.07	1.07 ± 0.10	0.82 ± 0.10	1.25 ± 0.19	1.28 ± 0.08	0.96 ± 0.32	0.95 ± 0.19
Cr_2O_3	57.90 ± 0.83	58.7 ± 1.3	56.9 ± 2.2	57.4 ± 1.7	58.3 ± 3.4	58.6 ± 1.1	57.7 ± 7.4	55.4 ± 9.1
TiO_2	2.34 ± 0.33	2.88 ± 0.20	2.94 ± 0.80	2.86 ± 0.52	1.46 ± 0.84	1.80 ± 0.83	2.6 ± 2.2	2.1 ± 1.9
Total	99.5	100.41	100.02	99.04	98.75	97.44	99.27	99.04
$MgAl_2O_4$ (spinel)	2.1 ± 0.2	2.7 ± 0.4	1.5 ± 0.3	1.3 ± 0.6	2.0 ± 2.5	1.4 ± 0.7	1.3 ± 1.1	2.9 ± 5.7
$FeAl_2O_4$ (hercynite)	11.0 ± 1.0	8.9 ± 0.4	11.0 ± 1.0	9.0 ± 1.0	11.4 ± 4.5	8.4 ± 2.7	9.1 ± 6.8	13.0 ± 14.0
$FeCr_2O_4$ (chromite)	70.1 ± 1.2	64.6 ± 2.6	72.8 ± 1.6	74.1 ± 5.1	70.7 ± 12.2	74.9 ± 5.1	76.1 ± 16.5	68.4 ± 19.9
$MgCr_2O_4$ (picrochromite)	13.8 ± 1.3	19.6 ± 2.7	10.0 ± 2.0	11.0 ± 4.0	13.3 ± 6.7	12.4 ± 1.9	9.3 ± 7.1	12.0 ± 3.4
Fe_2TiO_4 (ulvöspinel)	2.7 ± 0.4	3.0 ± 0.2	4.0 ± 1.0	3.5 ± 0.6	1.7 ± 0.9	2.2 ± 0.9	3.3 ± 2.7	2.5 ± 2.5
Mg_2TiO_4 (qandelite)	0.5 ± 0.1	0.9 ± 0.1	0.5 ± 0.2	0.5 ± 0.2	0.3 ± 0.3	0.4 ± 0.2	0.5 ± 0.4	0.4 ± 0.3
Fe_3O_4 (magnetite)	0.2 ± 0.6	0.4 ± 1.6	0.3 ± 1.7	0.5 ± 1.6	0.3 ± 0.8	0.3 ± 0.8	0.5 ± 0.9	0.4 ± 1.1

Mole % of spinel group end members: spinel, hercynite, chromite, picrochromite, ulvöspinel, qandilite and magnetite are calculated using End Member Generator (EMG) (Ferracutti et al., 2015).
[a] Refers to the total number of olivine grains analyzed in each sample.
[b] 2SD of the distribution of average grain compositions.
[c] All Fe expressed as FeO.

Table 3
Average temperature and range of temperatures derived from olivine-spinel thermometry.

Sample	Average temperature (°C)	Range of temperatures (°C)	No. of pairs
SaU 228 (H6)	704 ± 10 (15)	690–724	11
JaH 578 (H6)	865 ± 32 (10)	798–902	26
Dho 1012 (L6)	712 ± 35 (10)	635–767	23
AHu 017 (L6)	694 ± 23 (17)	648–719	9
SaU 246 (H3/4)	750 ± 88 (19)	660–895	7
RaS 337 (H3.6)	688 ± 27 (22)	679–715	5
RaS 265 (L3)	693 ± 51 (13)	617–811	14
JaH 596 (L3)	779 ± 64 (16)	658–834	10

Average temperature refers to the mean of the individual temperatures determined in each sample. The associated uncertainties shown in parenthesis are given in 2SD of the distribution of the average temperature.

the olivine-spinel pairs selected for thermometric calculations in each sample. Fig. 2 shows individual temperature values determined from each pair in each sample. Type 6 samples SaU 288, Dho 1012 and AHu 017 yield an average temperature of ~700 °C, which is in perfect agreement with previous temperature estimates for L6 and H6 samples (Sack and Ghiorso 1991b; Kessel et al., 2007; Wlotzka, 2005). However, a significantly higher average temperature of 865 ± 32 °C (2SD uncertainty based on multiple measurements in a single sample) is derived for sample JaH 578 (H6). In type 3 samples, RaS 337 (H3.6) gives an average temperature of 688 ± 27 °C. All the other type 3 samples, RaS 265 (L3), JaH 596 (L3) and SaU 246 (H3/4), give a relatively wider scatter of temperatures which reflects the unequilibrated nature of the olivine and spinel compositions in these samples, additionally supporting their low-metamorphic grade formation.

3.3. Mn/Cr ratio in chromite and silicate fractions

The Mn/Cr ratios of chromite and silicate fractions for all samples are listed in Table 4. The Mn/Cr ratios of silicate fractions range from 1.12 ± 0.02 to 4.13 ± 0.13 and show a bifurcation into unequilibrated (1.12 ± 0.02 to 2.18 ± 0.06) and equilibrated (2.13 ± 0.08 to 4.13 ± 0.13) chondrites (Fig. 3). Mn/Cr ratios of chromite fractions range from 0.0064 ± 0.0002 to 0.0108 ± 0.0002 with systematically higher Mn/Cr ratios in chromites from H chondrites (0.0093 ± 0.0002 to 0.0108 ± 0.0002) as compared to chromites in L chondrites (0.0064 ± 0.0002 to 0.0075 ± 0.0001) (Fig. 3). The Mn/Cr ratios of chromite fractions in the H chondrites are in good agreement with previously reported Mn/Cr ratios of chromite components in Dimmitt (H3/4) (Mn/Cr = 0.009 ± 5%) and Plainview (H5) (Mn/Cr = 0.011 ± 5%) chondrites (Lugmair and Shukolyukov,

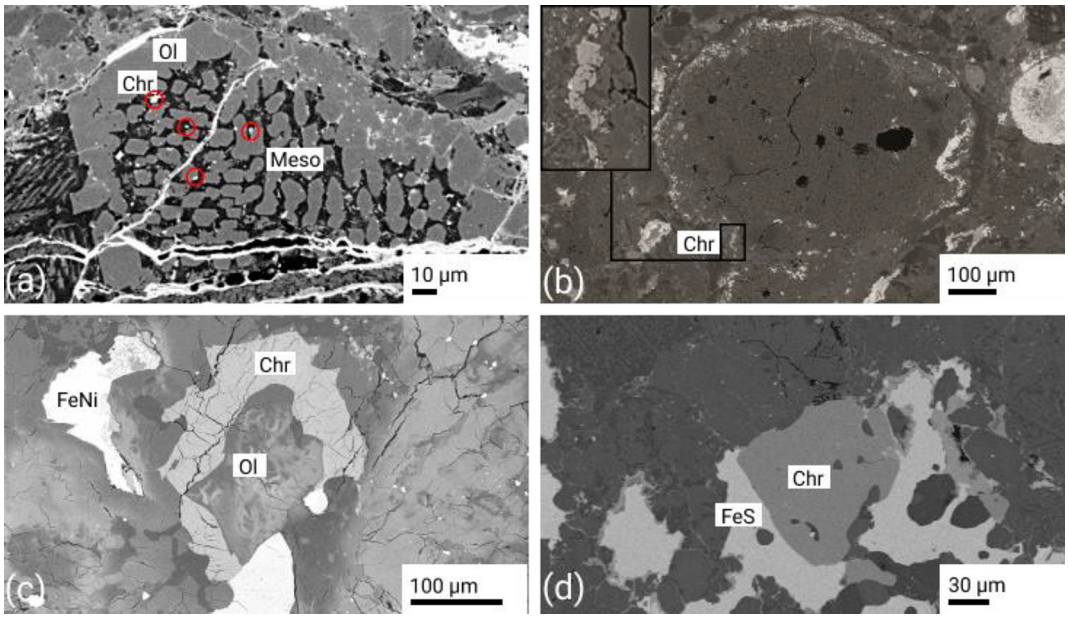

Fig. 1. Backscattered electron (BSE) images showing typical occurrences of spinel grains/aggregates in type 3 and type 6 ordinary chondrites (a) Cr-rich grains within olivine or between the grain boundaries of olivine and adjacent phases in a chondrule of sample JaH 596 (L3); (b) Spinel grains aggregating along the rim around a chondrule in sample RaS 337 (H3.6), inset shows an enlarged image of the spinel aggregate; (c, d) Spinel in close association with Fe-Ni metal, mafic silicates and troilite in the matrices of samples Dho 1012 (L6) and JaH 578 (H6). Chr = chromite; FeS = troilite; Ol = Olivine, Meso = mesostasis, Fe-Ni = Fe-Ni metal.

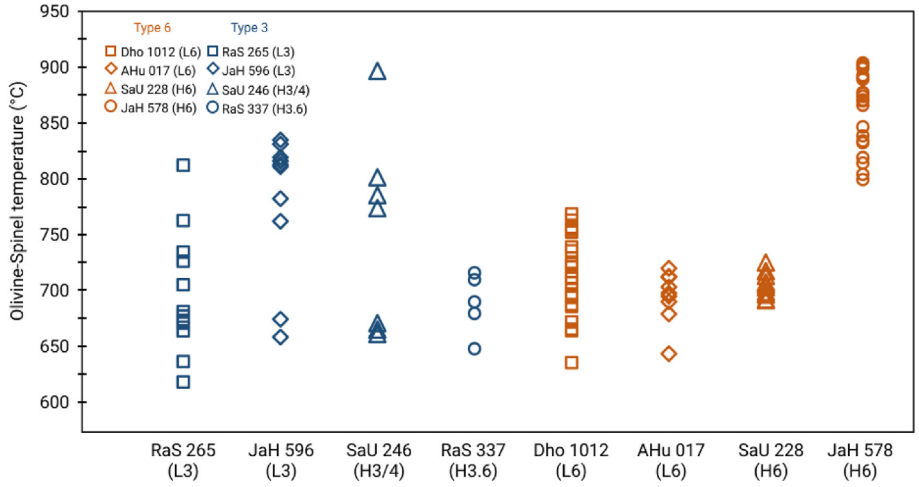

Fig. 2. Individual temperature values estimated with the olivine-spinel thermometer. Type 3 samples show a wider scatter of temperatures compared to type 6 samples due to incomplete equilibration of the phases. Significantly higher temperatures are derived for sample JaH 578 (H6) among all type 6 samples. Uncertainties associated with each temperature estimate are approximately ±50 °C (1σ) (Benedix et al., 2005) and are not shown for the sake of clarity.

1998). They also agree with the Mn/Cr = 0.01 ± 1% in the chromite component from meteorite sample Ste. Marguerite (H4) (Trinquier et al., 2008b). However, the Mn/Cr = 0.025 ± 5% for chromite in the L chondrite Finney (L5) reported in Lugmair and Shukolyukov (1998) is significantly higher than the range of Mn/Cr ratios in chromites from L chondrites analyzed in the present study. The range of Mn/Cr ratios for silicate fractions in the unequilibrated chondrites analyzed in the present study agrees within uncertainties with the Mn/Cr ratios for silicate components in Dimmitt (H3/4) (Mn/Cr = 1.73 ± 5%), Plainview (H5) (Mn/Cr = 2.45 ± 5%) and Finney (L5) (Mn/Cr = 2.45 ± 5%) meteorites (Lugmair and Shukolyukov, 1998).

3.4. Cr isotope compositions

The ε^{53}Cr of chromite and silicate fractions determined in all samples are listed in Table 4. The ε^{53}Cr of chromite

Table 4
Mn/Cr, Fe/Cr and Cr isotopic compositions of studied samples.

Sample	Fraction	Mn/Cr	2SE[a]	Fe/Cr	2SE[a]	ε^{53}Cr	2SE (n[a])	ε^{54}Cr	2SE
SaU 246 (H3/4)	Chromite	0.0098	0.0001	0.44	0.01	0.06	0.05(4)	−0.43	0.20
	Silicate	1.39	0.04	172.6	3.6	0.35	0.02(5)	−0.14	0.12
RaS 337 (H3.6)	Chromite	0.0095	0.0004	0.41	0.01	−0.02	0.03(2)	−0.40	0.01
	Silicate	1.69	0.03	215.6	2.0	0.43	0.02(4)	−0.10	0.14
JaH 578 (H6)	Chromite	0.0093	0.0002	0.43	0.01	0.11	0.03(8)	−0.41	0.07
	Silicate (UC)	3.24	0.15	399.2	17.3	0.77	0.03(4)	0.44	0.07
	Silicate (C)	–	–	–	–	0.50	0.03(4)	−0.41	0.08
SaU 228 (H6)	Chromite	0.0108	0.0002	0.44	0.02	0.09	0.05(4)	−0.62	0.22
	Silicate	4.13	0.13	556.5	17.5	0.43	0.03(5)	−0.24	0.04
JaH 596 (L3)	Chromite	0.0075	0.0001	0.46	0.01	−0.03	0.03(6)	−0.57	0.17
	Silicate	1.12	0.02	91.7	1.1	0.36	0.02(5)	−0.41	0.09
RaS 265 (L3)	Chromite	0.0064	0.0002	0.43	0.01	−0.01	0.03(5)	−0.49	0.07
	Silicate (UC)	2.18	0.06	209.4	4.6	0.58	0.02(5)	0.14	0.18
	Silicate (C)	–	–	–	–	0.38	0.02(3)	−0.49	0.18
Dho 1012 (L6)	Chromite	0.0074	0.0001	0.46	0.01	0.09	0.02(5)	−0.45	0.16
	Silicate	3.03	0.06	298.3	3.3	0.19	0.03(5)	−0.22	0.04
AHu 017 (L6)	Chromite	0.0073	0.0002	0.44	0.01	0.05	0.04(4)	−0.59	0.16
	Silicate	2.13	0.08	203.7	6.3	0.25	0.03(5)	−0.28	0.08

The uncertainties associated with Mn/Cr, Fe/Cr, and Cr isotopic compositions are given in 2SE of the replicate measurements. See Supplementary Table S2 for Cr isotopic compositions of the individual runs. Cr isotopic compositions in the silicate fractions of samples RaS 265 and JaH 578 are reported after correction for spallogenic reactions. (C): corrected, (UC): uncorrected.
[a] Number of replicates measured for each sample.

fractions range from -0.02 ± 0.03 to 0.11 ± 0.03. The chromite fractions from L3 samples JaH 596 and RaS 265 record an average ε^{53}Cr of -0.02 ± 0.02 (2SD). In case of H3 samples, RaS 337 gives an ε^{53}Cr = -0.02 ± 0.03 in agreement with that of L3 samples. Chromite fraction in sample SaU 246 (H3/4) has a higher ε^{53}Cr (=0.06 ± 0.05) than chromite fractions from all the other type 3 samples. It agrees within uncertainties with the average ε^{53}Cr (0.09 ± 0.04, 2SD) determined in chromite fractions from type 6 samples. The ε^{53}Cr in silicate fractions range from 0.19 ± 0.03 to 0.77 ± 0.03 and agree within uncertainties with previously reported ε^{53}Cr for silicate fractions in ordinary chondrites, such as $\varepsilon^{53}\text{Cr} = 0.59 \pm 0.10$, 0.65 ± 0.13 and 0.52 ± 0.10 for samples Dimmitt (H3,4), Plainview (H5) and Finney (L5), respectively (Lugmair and Shukolyukov, 1998).

3.5. Correction for spallogenic Cr

Spallation reactions induced by cosmic-ray exposure (CRE) can alter ^{53}Cr/^{52}Cr ratios in solar system objects. This alteration depends on the duration of cosmic ray exposure, its intensity, Fe/Cr ratio and shielding condition for any given sample and requires a correction before the Cr isotope systematics can be used as a dating tool (Liu et al., 2019). Fig. 4 shows an ε^{54}Cr vs ε^{53}Cr diagram for the chromite and silicate fractions of all samples. Due to significantly high radiogenic ε^{53}Cr and low Fe/Cr ratios in the chromite fractions, cosmogenic contributions are negligible and hence no correction is needed. However, silicate fractions with higher Fe/Cr ratios may require correction for spallogenic Cr (Table 4). Since chromite and silicate fractions formed from the same reservoir and the correlation between ε^{53}Cr and ε^{54}Cr is unaffected by the spallogenic reactions (Liu et al., 2019), ε^{54}Cr of the chromite fractions can be used to internally correct the Cr isotopic composition of the silicate fractions. From Fig. 4 such correction appears necessary in samples RaS 265 and JaH 578 that show ε^{54}Cr values remarkably higher than the mean ε^{54}Cr found in ordinary chondrites (whole rock and components), compiled from the literature (Trinquier et al., 2007, 2008b; Qin et al., 2010; Schneider et al., 2020). To reconcile the ε^{54}Cr values of the silicate fractions of samples RaS 265 and JaH 578 with their chromite fractions, the Cr isotopic compositions are corrected using the equation given in Table 2 in Trinquier et al. (2007) and a ^{53}Cr and ^{54}Cr production rate of 2.9×10^{11} atoms/Ma in Fe targets (Birck and Allègre, 1985b). The correction estimates a CRE age of 237 Ma for RaS 265 and 169 Ma for JaH 578. The corrected ε^{53}Cr and ε^{54}Cr are reported in Table 4.

3.6. Chromite model ages

The evolution of ε^{53}Cr in a chondritic reservoir as expressed by Eq. (1) is used to derive model ages from the chromite fractions. The model ages are calculated relative to the CAI formation age of 4567.18 ± 0.50 Ma (Amelin et al., 2010) assuming solar system initial $\varepsilon^{53}\text{Cr} = -0.23$, CI chondritic ^{55}Mn/^{52}Cr = 0.71 and a canonical $^{53}\text{Mn}/^{55}\text{Mn} = 6.28 \times 10^{-6}$ (Trinquier et al., 2008b). These ages are reported in Table 5 and plotted on the chondritic ε^{53}Cr evolution diagram (Fig. 5).

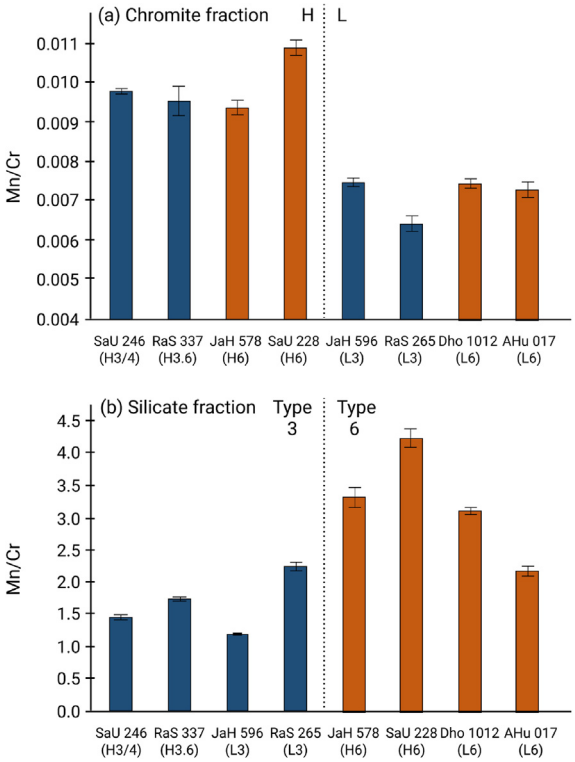

Fig. 3. (a) Mn/Cr ratios in chromite fractions. The ratios are systematically higher in H chondrites than L chondrites (b) Mn/Cr ratios in silicate fractions. The dashed line highlights the dichotomy between lower Mn/Cr ratios in type 3 samples and higher Mn/Cr ratios in type 6 samples. Uncertainties associated with the Mn/Cr ratios determined by replicate measurements are shown as 2SE.

The chromite model ages correlate with the petrologic grade of the samples and yield two distinct "clusters" (Fig. 5). The first cluster comprises samples RaS 337 (H3.6), JaH 596 (L3) and RaS 265 (L3), all of which are of petrologic type 3 and yield model ages from $3.99^{+0.93}_{-0.79}$ Ma to $4.51^{+1.10}_{-0.91}$ Ma after CAI formation. The chromite fraction from sample SaU 246 (H3/4) displays a younger age ($7.4^{+3.4}_{-2.1}$ Ma) than the chromites from other type 3 samples. It lies closer to the second cluster that comprises all the type 6 samples. The model ages for the second cluster range from $6.9^{+2.1}_{-1.5}$ Ma to$11.1^{+6.0}_{-2.8}$ Ma. There is no systematic difference in model ages for both H and L chondrites, therefore they are discussed together assuming similar structures, sizes, accretion time and high-temperature cooling histories of their parent bodies.

3.7. Isochron ages

In addition to the chromite model ages, two-point isochron ages are obtained from pairs consisting of chromite and corresponding silicate fractions from each sample. Fig. 6(a)–(h) illustrates the data from Table 4 for each chondrite sample. The ε^{53}Cr and ^{55}Mn/^{52}Cr data are used to construct two-point isochrons by regression in IsoplotR (Vermeesch, 2018) taking the maximum likelihood regression model. The use of two-point isochrons is justified for these samples because the chromites formed from their surrounding matrix and thus both components had the same initial Cr-isotope composition when the chromite grew. This is similar to the approach commonly used in meteorite studies where only two components can be used to obtain a significant spread in isotope space (e.g., Birck and Allègre, 1988). The slope of the isochron then yields the initial ^{53}Mn/^{55}Mn ratio of the sample at the time of Mn-Cr fractionation. Comparison of this isotope ratio with ^{53}Mn/^{55}Mn = $2.59 \pm 0.34 \times 10^{-6}$ at the time of isotopic closure in the carbonaceous achondrite NWA 6704 (Sanborn et al., 2019) yields the age of thermal metamorphism of the sample relative to NWA 6704. The inferred initial ^{26}Al/^{27}Al$_0$ = 3.15 ± 0.38 × 10^{-7} of NWA 6704 (Sanborn et al., 2019) and corresponding ^{26}Al-^{26}Mg age of 5.2 ± 0.2 Ma relative to the canonical ^{26}Al/^{27}Al$_0$ value of CAIs (Jacobsen et al. 2008; Larsen et al., 2011), is used to calculate the Mn-Cr age of the samples relative to the CAI formation. The ^{53}Mn/^{55}Mn ratios and two-point isochron ages for each sample are reported along with the chromite model ages in Table 5. The table also includes reported isochron ages for equilibrated ordinary chondrites.

4. DISCUSSION

4.1. The onset and progression of metamorphism in ordinary chondrites

Spinel group minerals have widely been used to study the onset and progressive thermal metamorphism in ordinary chondrites (e.g., Johnson and Prinz, 1991; Grossman and Brearley, 2005, Kimura et al., 2006). Kimura et al. (2006) studied LL3.0-LL6 chondrites and reported multiple origins and formation mechanisms of spinel group minerals, especially in type 3.0–3.9 ordinary chondrites. The authors showed that the occurrence of nearly pure chromite and a wide compositional variation can distinguish spinel group minerals in types 3.0–3.3 from those in the other types. Spinel group minerals in types 3.5–3.9 show a narrower range of compositions, and those in types 4–6 are homogeneous. Most of the spinel group minerals in chondrules of type 3.0–3.3 crystallized from the chondrule melt and give olivine-spinel temperatures of ≥1000 °C, reflecting chondrule crystallization conditions (Johnson and Prinz, 1991). The two L3 samples, JaH 596 and RaS 265, investigated in the present study show olivine-spinel temperatures within the range of 620–830 °C which is typical of type 3.5–3.9 samples. Such low temperatures reflect either reset or formation during progressive thermal metamorphism.

Thermal metamorphism can produce chromite grains by exsolution of Cr incorporated into olivine at higher temperature. The onset of thermal metamorphism in ordinary chondrites leads to the chemical homogenization of olivine and eventually a decrease in its Cr-content (Grossman and Brearley, 2005). This equilibration can be observed starting as early as in petrologic type 3.0–3.3. (McCoy et al., 1991, DeHart et al., 1992). Grossman and Brearley (2005) found a Cr-rich phase, <1 μm large, exsolving from olivine in type L3.10 chondrites. Similar sub-μm Cr-rich grains within oli-

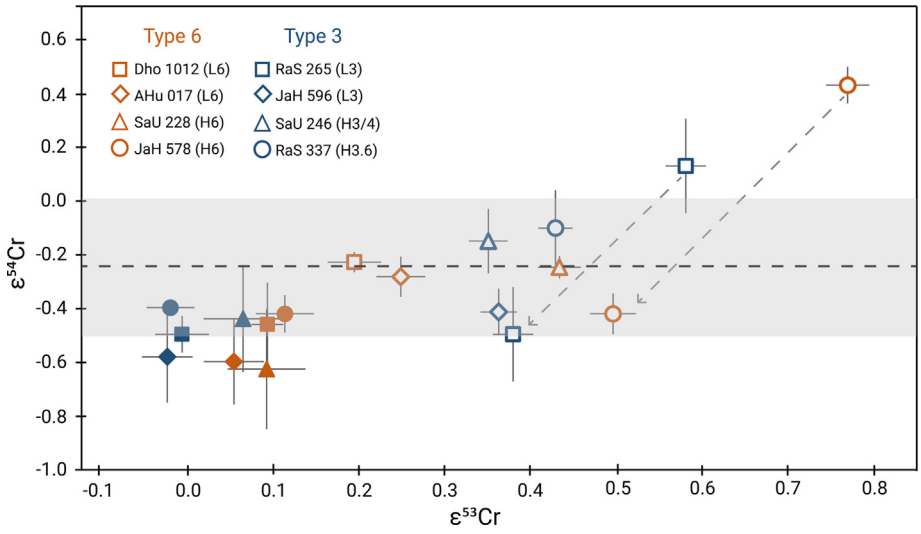

Fig. 4. ε^{53}Cr vs ε^{54}Cr diagram for the chromite and silicate fractions from the studied samples. The shaded region represents the mean and 1 standard deviation (=−0.24 ± 0.26) of the ε^{54}Cr in ordinary chondrites (whole rock and components), compiled from the literature (Trinquier et al., 2007, 2008b; Qin et al., 2010; Schneider et al., 2020). The dashed arrows show the correction applied for spallogenic Cr in samples RaS 265 and JaH 578 (see text).

Table 5
Chromite model ages and two-point isochron ages determined for the studied chondrites.

Sample	Chromite model age (Ma after CAIs)	isochron ages		
		^{53}Mn/^{55}Mn	2σ	Age (Ma after CAIs)
This study				
SaU 246 (H3/4)	$7.4^{+3.4}_{-2.1}$	2.35 × 10^{-6}	0.43 × 10^{-6}	$5.60^{+1.08}_{-0.90}$
RaS 337 (H3.6)	$4.10^{+0.89}_{-0.76}$	3.03 × 10^{-6}	0.24 × 10^{-6}	$4.24^{+0.44}_{-0.41}$
JaH 578 (H6)	$11.1^{+6.0}_{-2.8}$	1.34 × 10^{-6}	0.16 × 10^{-6}	$8.62^{+0.70}_{-0.62}$
SaU 228 (H6)	$9.2^{+5.4}_{-2.6}$	9.41 × 10^{-7}	1.48 × 10^{-7}	$10.54^{+0.92}_{-0.79}$
JaH 596 (L3)	$3.99^{+0.93}_{-0.79}$	3.96 × 10^{-6}	0.39 × 10^{-6}	$2.78^{+0.55}_{-0.50}$
RaS 265 (L3)	$4.51^{+1.10}_{-0.91}$	2.02 × 10^{-6}	0.21 × 10^{-6}	$6.43^{+0.61}_{-0.55}$
Dho 1012 (L6)	$9.3^{+1.6}_{-1.3}$	3.80 × 10^{-7}	1.35 × 10^{-7}	$15.4^{+2.4}_{-1.6}$
AHu 017 (L6)	$6.9^{+2.1}_{-1.5}$	1.04 × 10^{-6}	0.24 × 10^{-6}	$10.0^{+1.4}_{-1.1}$
Literature				
Finney (L5)[a]	–	2.70 × 10^{-7}	–	~17.20
Ste. Marguerite (H4)[b]	–	2.78 × 10^{-6}	0.46 × 10^{-6}	4.7 ± 1.0

Uncertainties on the model ages are determined using uncertainties on ε^{53}Cr values of the samples. ^{53}Mn/^{55}Mn ratio refers to the slope of the two-point isochron. Associated error on slope is given at 2σ level. Uncertainties on two-point isochron ages are determined using uncertainties on ^{53}Mn/^{55}Mn ratios. Sources for literature data: (a) ^{53}Mn/^{55}Mn and corresponding isochron age for Finney (L5) is determined by regression in IsoplotR (Vermeesch, 2018) using ε^{53}Cr of silicate, whole rock and chromite fractions reported in Lugmair and Shukolyukov (1998) and anchored to achondrite NWA 6704 (b) ^{53}Mn/^{55}Mn for Ste. Marguerite (H4) is taken from Trinquier et al. (2008b) and corresponding isochron age is determined by anchoring to NWA 6704 (see text).

vine or between the grain boundaries of olivine and adjacent phases are also observed in chondrules of sample JaH 596 (L3) and RaS 265 (L3) (Fig. 1a) and inferred to be chromite. With increasing metamorphic grade, such small grains coalescence to form larger chromite grains, first aggregating along the rim around chondrules as seen in SaU 246 (H3/4) and RaS 337 (H3.6) (Fig. 1b), and then becoming equant phases in the matrix of type 6 samples (Fig. 1c, d). In addition to the crystallization from the chondrule melt or formation due to thermal metamorphism, relic origin of spinel in chondrule is also identified (Kimura et al., 2006). These 5–35 μm spherical to irregular

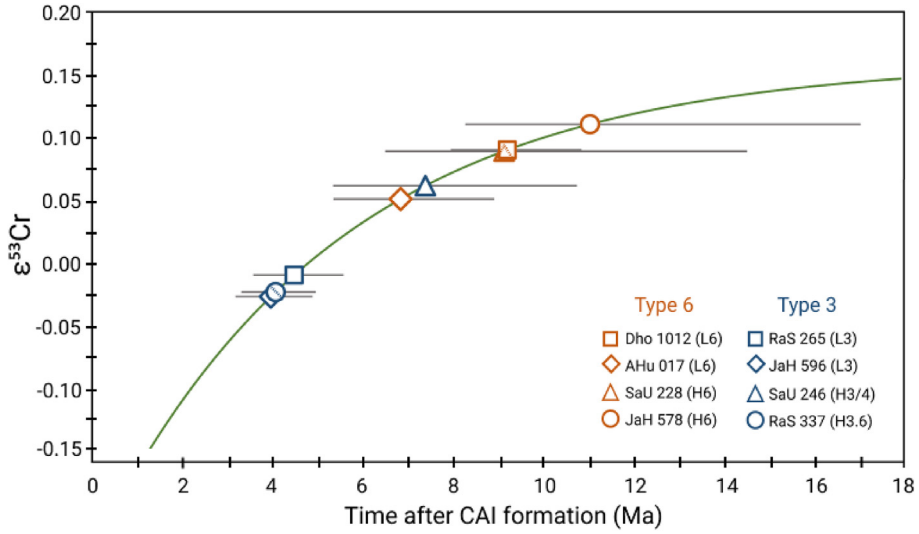

Fig. 5. The model ages are plotted on a curve representing the ε^{53}Cr evolution of the chondritic reservoir through time. Uncertainties on the model ages are determined using uncertainties on the ε^{53}Cr values of the samples. The model ages correlate with the petrologic grade of the samples and yield two distinct "clusters". The first cluster comprises type 3 samples except sample SaU 246 (H3/4) that lies closer to the second cluster that comprises type 6 samples.

gains that survived the melting of the chondrule precursor materials were described in LL3.15-LL3.3 chondrites (Kimura et al., 2006), however, not observed in type 3 samples investigated in the present study; indicating the possibility of their higher petrologic subgrade.

The chemical equilibration of olivine and newly formed chromite commenced with the exsolution of chromite grains at the onset of thermal metamorphism and continued with the inter-and intragrain homogenization of the olivine crystals. Chemical equilibration is evident in the studied samples when comparing the abundance and chemistry of chromite grains in type 3 and type 6 samples. The gradual equilibration of spinel and its reactivity during prograde metamorphism is also reflected in the result of the olivine-spinel thermometry. Type 3 samples yield a relatively wider range of temperature estimate in individual samples (Fig. 2) as compared to type 6 samples. The olivine-spinel temperatures in type 6 samples show chemical homogenization and equilibration of the phases acquired at higher metamorphic temperature. Kessel et al. (2007) studied equilibrated type 4–6 chondrites from H, L and LL classes applying olivine-spinel thermometry and showed that the maximum temperatures (interpreted as equilibration temperatures) recorded by individual chondrites increase subtly, but systematically with the metamorphic type and are tightly clustered. They observed a correlation between the spinel grain sizes and the determined temperatures: larger spinel grains are resistant and preserve the peak temperature above the closure temperature of the Fe-Mg diffusion in olivine-spinel pairs, while smaller spinel grains continued to re-equilibrate during retrograde metamorphism, recording a range of lower closure temperatures. Wlotzka (2005) incorporated "unequilibrated" type 3.7 and 3.8 chondrites and for the first-time calculated temperatures, that can be interpreted as "equilibrium temperatures" for these samples. Wlotzka (2005) argued that subtypes 3.7–3.9 are already partially equilibrated by a Fe-Mg exchange between Fe-Mg silicates and Cr-spinel and thus temperatures derived from the olivine-Cr-spinel pairs represent equilibrium temperatures. Sample RaS 337 (H3.6) gives an average temperature value of 688 °C which is within the temperature range of 619–699 °C (Fig. 2) reported by Wlotzka (2005) for type H3.7–3.8 samples.

4.2. Closure temperature of the Mn-Cr system in spinel

The interpretation of Mn-Cr isochron and chromite model ages requires estimates for the diffusivity of Cr in different minerals as a function of temperatures. Chromium diffusion data are available for olivine (Ito and Ganguly, 2006), orthopyroxene (Ganguly et al., 2007) and chromite (Posner et al., 2016). The Mn-Cr isochron ages for several H and L chondrites have been investigated in previous studies (e.g., Lugmair and Shukolyukov, 1998) and mostly rely on whole rock, chromite and silicate fractions. However, the silicates with high Mn/Cr ratios dominate the slope and the resulting age. Due to uncertainties concerning which phase dominates the Mn budget and, hence, which closure temperature should be applied, the Mn-Cr chondrite cooling ages are generally ignored in the thermal history models to constrain the metamorphic evolution of ordinary chondrite parent bodies (Henke et al., 2013). Unlike the Mn-Cr isochron, the chromite model ages require a Cr closure temperature estimate in chromite only and this information is crucial for a meaningful interpretation of chromite model ages, i.e., whether they date the time of mineral growth or some time along the cooling path.

For any mineral, the closure temperature depends on the diffusion behavior as a function of temperature, cooling rate, and effective diffusion radius; the latter can be related

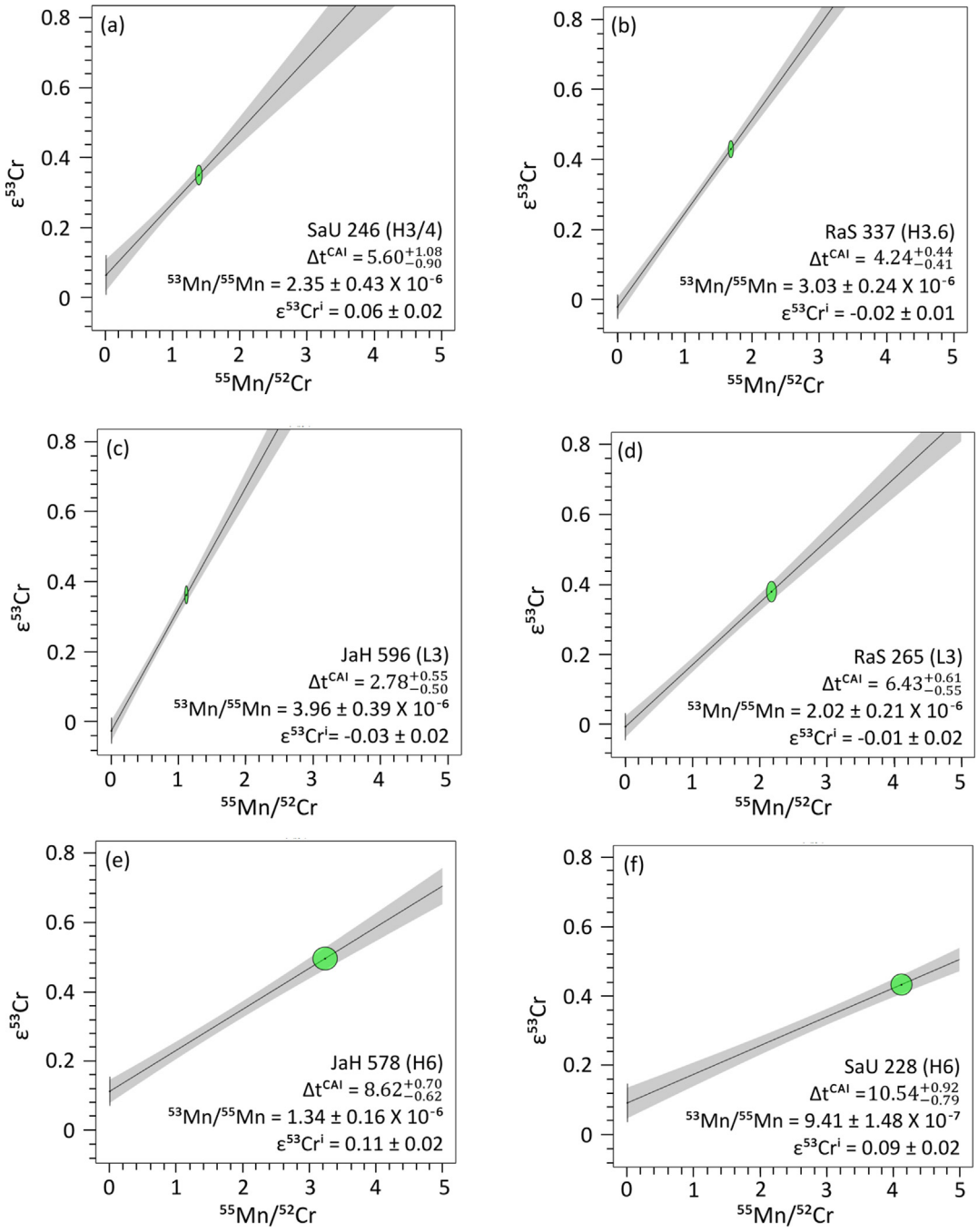

Fig. 6. (a-h) $\varepsilon^{53}Cr$ vs $^{55}Mn/^{52}Cr$ diagrams for the studied sample. The $\varepsilon^{53}Cr$ and $^{55}Mn/^{52}Cr$ data points for the chromite and silicate fractions in each sample are used to construct a two-point isochron. Δt^{CAI} refers to formation interval relative to CAIs.

to the grain size (Dodson, 1973). Sugiura and Hoshino (2003) investigated Mn-Cr systematics in phosphates (sarcopside, graftonite, beusite, galileiite and johnsomervilleite) by secondary ion mass spectrometry (SIMS) in the slowly cooled IIIAB iron meteorites. They observed that the different phosphate phases yield different "ages" due to different Mn-Cr diffusion rates, and thus different closure temperatures. Only in rapidly cooled systems, where parent and daughter elements do not diffuse significantly, does the age correspond to the time of mineral formation and approximates the growth age of the phase. Since IIIAB iron meteorites cooled slowly at a rate of ca. 60–200 °C/Ma (e.g., Matthes et al., 2020), the Mn-Cr chronometer does not provide the time of formation of minerals in IIIAB iron meteorites but the time of "closure" (i.e. the time at which the Mn-Cr system was frozen, Sugiura and Hoshino 2003), which can be different for different minerals.

Recently, Sievwright et al. (2020) reported that the diffusion coefficients of a wide range of cations in magnetite increase in the order: Cr < Mo ≈ Ta < V < Ti

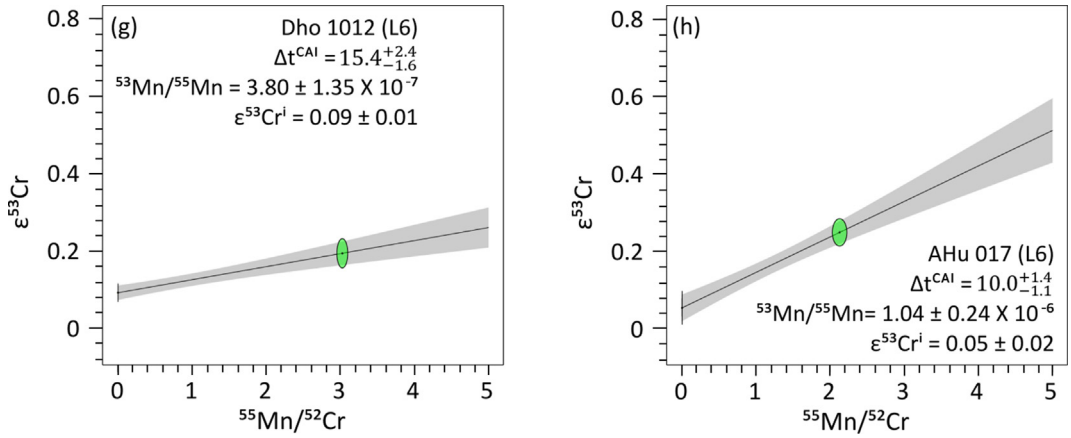

Fig. 6 (*continued*)

<Al<Hf≈Nb<Sc≈Zr≈Ga<In<Lu≈Y<Ni<U≈Zn<Mn≈Mg < Co < Li < Cu. Isostructural with magnetite, the order should also hold for chromite. The assumed relatively low diffusion coefficient of Cr in chromite implies that the original content of Cr should be well preserved.

Posner et al. (2016) carried out a tracer diffusion experiment of Cr in natural spinels at 1 bar and 950–1200 °C under controlled $f(O_2)$ conditions to determine the dependence of the Cr diffusion coefficient D(Cr) and closure temperature on $f(O_2)$ and Cr# (i.e., Cr/(Cr + Al)). They used the closure temperature calculator developed by Ganguly and Tirone (2009) as an extension of the classic work of Dodson (1973) to calculate closure the temperature of Cr in spinel as a function of (i) peak temperature, (ii) grain size, (iii) cooling rate and (iv) $f(O_2)$. This calculator is used in the present study to constrain the closure temperature of Cr in spinel from type 3 and 6 ordinary chondrites. The results are shown in Fig. 7.

For type 6 ordinary chondrites, a temperature of ca. 1000 °C provides an upper limit for the possible peak temperature since the beginning of melting in chondritic material would be the eutectic melting in the FeNi-FeS system at ~1000 °C, but ordinary chondrites lack any indications for partial melting (Gail and Trieloff, 2019). Two-pyroxene thermometry (Lindsley and Andersen, 1983) provides peak temperature estimates of 865–926 °C for H6 and 812–934 °C for L6 chondrites (Slater-Reynolds and McSween, 2005). Schrader et al. (2016) investigated the compositional and textural evolution of sulfides within a wide range of thermally metamorphosed LL chondrites and reported peak temperatures of ~900 °C. The peak metamorphic temperatures in type 3 chondrites are poorly constrained because of the unequilibrated composition of phases which negates the rigorous application of commonly used geothermometers. Dodd (1981) estimated a peak temperature range of 400–600 °C for type 3 chondrites. Further work on type 3 meteorites determined a wider range of peak temperatures from 260 to 600 °C (e.g., Huss et al., 2006, Busemann et al., 2007). Wlotzka (2005) used the olivine-spinel thermometer and derived an "equilibrium temperature" of 619–699 °C for H3.7–3.8 chondrites. Subtypes within type 3 s were found to correlate well with the estimated peak temperatures. Wlotzka (2005) furthermore argued that the equilibrium temperature may not necessarily be the peak temperature experienced by chondrites, but for type 3.7–3.8, it was not exceeded by more than 100 °C for a long time. Otherwise, they would have been equilibrated to type 4. A comparison between the thermal model of H (Henke et al., 2012b, 2013) and L (Gail and Trieloff, 2019) chondrite parent bodies shows that the peak temperature reached at the burial depths of H6 meteorites is ~50 °C higher than that in L6 meteorites. Nevertheless, considering the maximum temperature of ~930 °C (Slater-Reynolds and McSween, 2005) deduced from two-pyroxene thermometry in type 6 meteorites of both H and L meteorites, it is reasonable to assume a maximum temperature of ~1000 °C for the calculation of Cr closure temperature in spinel of type 6 meteorites (H/L). In case of type 3 meteorites, a peak temperature of ~600 °C at the burial depth of type 3–4 transition derived from the thermal models is assumed to be the peak temperature for type 3 meteorites (H/L). However, it could be higher for type 3.7–3.8, but to what extent is unknown.

Fig. 7 shows the calculated closure temperatures of Cr in spinels as a function of cooling rate, grain size (=taken as effective diffusion radius) and maximum temperature of class H and L ordinary chondrites. For the model it is assumed that the peak temperature was 1000 °C, Cr# = 0.85 and grain sizes range from 2.5 to 300 μm. Posner et al. (2016) calculated D(Cr) and closure temperature at Cr# = 0 and 1 using a linear variation in logD(Cr) with Cr# ($d\log D(Cr)/dCr\# = 0.08$) as shown by Suzuki et al. (2008). This linear variation in logD(Cr) and Cr# is used in the present study to calculate D(Cr) at Cr# = 0.85 which has been reported as the mean Cr# in H, L and LL chondrites (e.g., Wlotzka, 2005). The grain sizes of spinel in type 6 samples are reported to range from 50 to 150 μm (Kimura et al., 2006, Kessel et al., 2007). Much smaller spinel grains are observed in type 3 samples, ranging from ~1 to 10 μm (Kimura et al., 2006).

The cooling rates of ordinary chondrites are the subject of an ongoing debate. Ganguly et al. (2013, 2016) devel-

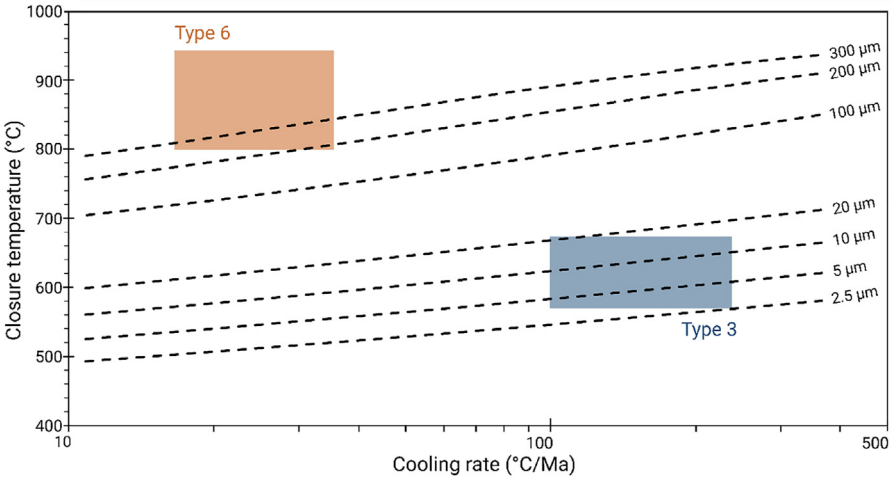

Fig. 7. Closure temperature of the Mn-Cr system in spinel grains. The dashed lines represent the closure temperature curves as a function of initial temperature (=1000 °C) at the onset of cooling and grain size (effective diffusion radius). The metamorphic peak temperature ranges for type 3 and 6 ordinary chondrites are constrained by the closure temperature curves and respective typical cooling rates (coloured boxes). Details regarding the calculations are given in the text. (For interpretation of the references to colour in this figure legend, the reader is referred to the web version of this article.)

oped a multistage cooling model for H, L and LL chondrites. They measured the composition of coexisting mineral phases in several type 4 to 6 chondrites and derived high-temperature cooling rates of ~25–100 °C/ka at high temperatures, commencing from 750-850 °C. At lower transitional temperatures (500–450 °C), an average cooling rate of ~15 °C/Ma was estimated from the Fe-Mg ordering states of orthopyroxenes. Hellmann et al. (2019) estimated the cooling rates in type 5 and 6 chondrites by Hf-W chronology of coarse-grained metals that plot below the isochrons defined by silicate-dominated fractions. These samples yield cooling rates between 2 and 28 °C/Ma. For those type 5 and 6 samples where metal and silicate-dominated fractions define a single Hf-W isochron, a lower limit on the cooling rate of 30–54 °C/Ma was determined. Cooling rates for type 3 chondrites are poorly constrained. Kleine et al. (2008) obtained cooling rates from the slopes of cooling curves for type 4–6H chondrites. Assuming an onion shell model for the chondrite parent bodies which predicts an inverse correlation of cooling rates with petrologic type, a cooling rate of ~100 °C/Ma for type 4 meteorites, can thus be considered a lower limit for the cooling rate of type 3 samples.

From Fig. 7, a Cr closure temperature of ~760 °C is deduced for spinel from type 6 chondrites assuming Cr# = 0.85, grain size = 150 µm and a cooling rate of ~30 °C/Ma. A closure temperature ~760 °C in type 6 samples is likely a lower limit since, at higher transitional temperatures, the cooling rate would be higher which in turn, would result in higher closure temperatures. In type 3 chondrites, Cr closure temperature is estimated to be ~540–620 °C, for a spinel grain size between 5 and 10 µm and a cooling rate of 100–150 °C/Ma.

The Mn-Cr model ages and closure temperature estimates can be compared with the Hf-W and ^{207}Pb-^{206}Pb ages and corresponding closure temperatures for respective petrological types of ordinary chondrites to constrain the thermal evolution of the respective parent bodies. The lower limit on Mn-Cr closure temperature of ~760 °C for type 6 ordinary chondrites is ~100 °C lower than the estimated Hf-W closure temperature (875 ± 75 °C) for H6 chondrites (Kleine et al., 2008). However, the Hf-W ages for type 5 and 6 chondrites (9.3 ± 1.3 Ma, 2SE, n = 11) determined by Hellmann et al. (2019) are in good agreement with Cr model ages obtained for type 6 chondrites (9.1 ± 1.5 Ma) in the present study. The agreement in the ages calculated by both the chronometers argues for a similar closure temperature for both systems, at least in type 6 samples. ^{207}Pb-^{206}Pb ages provide an additional check for the accuracy and significance of Mn-Cr ages and closure temperatures. The ^{207}Pb-^{206}Pb phosphate ages for type 5 chondrites range up to ~60 Ma after CAI formation (Blackburn et al., 2017). The closure temperature for Pb diffusion in phosphates is estimated to be ~530 °C (Cherniak et al., 1991) which is significantly lower than the closure temperature estimates for both Hf-W and Mn-Cr in type 6 chondrites. The younger ages and lower closure temperature for the ^{207}Pb-^{206}Pb system support the interpretation of the older ages and higher closure temperature for the Mn-Cr system determined in the present study. The Hf-W ages for type 4 chondrites range from 3.4 ± 0.7 to 4.3 ± 0.9 Ma (Hellmann et al., 2019) and are in good agreement with the Mn-Cr model ages ($3.99^{+0.93}_{-0.79}$ Ma to $4.51^{+1.10}_{-0.91}$ Ma) for type 3 chondrites determined in the present study. The closure temperature of the Hf-W system in H4 chondrites is ~800 ± 50 °C (Kleine et al., 2008), which is higher than the peak metamorphic temperature in type 4 chondrites. The Mn-Cr closure temperature is similar to the peak temperatures determined for type 3 chondrites. Consequently, Hf-W and Mn-Cr should both date the time of peak metamorphism in type 3–4 chondrites. The agreement in the ages determined by both the system provides

strong confidence in the chromite model ages calculated in the present study which are interpreted to date chromite formation.

4.3. Significance of initial $^{53}Cr/^{52}Cr$ and ^{53}Mn abundances for chromite model ages

To derive chromite model ages using Eq. (1), the solar system initial $^{53}Cr/^{52}Cr$ and canonical $^{55}Mn/^{52}Cr$ at a given time have to be known and assumed to be homogenous. The model ages reported in the present study are determined using initial $\varepsilon^{53}Cr$ = -0.23 and a canonical $^{53}Mn/^{55}Mn = 6.28 \times 10^{-6}$ (Trinquier et al., 2008b) (Table 5). Using $^{53}Mn/^{55}Mn_i = 7.68 \times 10^{-6}$ as recalculated from Ste. Marguerite systematics with the updated U-corrected ^{207}Pb-^{206}Pb phosphate age (Trinquier et al. 2008b; Blackburn et al. 2017), yields a mean age of ~4.5 Ma for type 3 samples and ~8.4 Ma (after CAIs) for type 6 samples, however, with much lower $\varepsilon^{53}Cr_i = -0.29$. Different studies have reported resolvable variations in the solar system initial $\varepsilon^{53}Cr$ and $^{53}Mn/^{55}Mn$ values as summarized in Section 2.1. Since the chromite model ages are strongly affected by the model parameters, clearly, more high-precision Cr isotope data to tightly constrain the initial $\varepsilon^{53}Cr$ and $^{53}Mn/^{55}Mn$ are needed. Using the solar system initial $\varepsilon^{53}Cr = -0.177$ and canonical $^{53}Mn/^{55}Mn = 6.8 \times 10^{-6}$ determined by Göpel et al. (2015) results in chromite model ages for type 3–6 chondrites ranging from, $2.39^{+0.62}_{-0.56}$ Ma to $6.2^{+1.5}_{-1.2}$ Ma after CAI formation (See Supplementary Fig. SF2). These ages predate the model ages of $3.99^{+0.93}_{-0.79}$ Ma to $11.1^{+6.0}_{-2.8}$ Ma determined using initial ^{53}Cr and ^{53}Mn abundances as reported in Trinquier et al. (2008b). The older model ages determined using the initial $\varepsilon^{53}Cr$ and $^{53}Mn/^{55}Mn$ values from Göpel et al. (2015) do not agree with the two-point isochron ages for type 3 and type 6 samples (Fig. 6). Moreover, the older model ages for type 3 samples predate the youngest chondrule formation ages in ordinary chondrites which are as late as ~2.9 Ma (Pape et al., 2019) after CAI formation. Since type 3 samples represent the last aggregating material on the ordinary chondrite parent bodies and have Cr closure temperatures similar to the peak metamorphic temperature, the model ages cannot be older than the youngest chondrule formation ages. Kleine et al. (2008) reported a Hf-W isochron age of 1.7 ± 0.7 Ma for the H4 chondrite Ste. Marguerite, which is older than the youngest chondrule formation age of ~2.9 Ma (Pape et al., 2019). The age was interpreted as the timing of chondrule formation and not attributed to the thermal processes on the parent body. The Hf-W isochron age for Ste. Marguerite was later updated to 3.8 ± 0.6 Ma after CAI formation (Hellmann et al. 2019), which postdates the chondrule formation interval.

Altogether, the initial $\varepsilon^{53}Cr$ (=−0.23) and ^{53}Mn (=6.28×10^{-6}) abundances reported in Trinquier et al. (2008b) produce a consistent data set for the chromite model ages that match with the Mn-Cr isochron ages in early solar system materials.

The Mn-Cr model ages reported in Table 5 are calculated assuming that chondrites represent an isotopically homogeneous reservoir that evolved with a distinct Mn/Cr ratio which is identical to CI chondrites (Birck et al., 1999). The assumption of CI-like compositional reservoir has proved to be valid, as the chromite model ages determined using a CI-like Mn/Cr = 0.71 are within uncertainties of the two-point isochron ages in the studied samples that did not reach thermal conditions above the closure temperature. A compilation of the Mn/Cr ratios (Wasson and Allemeyn, 1988; Trinquier et al., 2008b; Qin et al., 2010; Pedersen et al., 2019) reported for ordinary chondrites gives Mn/Cr = 0.73 for H chondrites and 0.77 for L chondrites. Using Mn/Cr = 0.73 results in slightly younger model ages compared to those calculated for a CI-like Mn/Cr. For instance, the model age for type 3 sample JaH 596 and type 6 sample AHu 017 would become $3.83^{+0.87}_{-0.75}$ Ma and $6.5^{+1.8}_{-1.4}$ Ma instead of $3.99^{+0.93}_{-0.79}$ Ma and $6.9^{+2.1}_{-1.5}$ Ma, respectively. These shifts are within the overall uncertainty of the model ages.

4.4. Chromite model ages vs. two-point isochron ages

Unlike chromite model ages, which are derived from chromite solely, two-point isochrons calculated in the present study involve chromite as well as the remaining silicate-metal bulk fraction of the same whole-rock meteorite. Isochrons based on analyses of different phases or components in a sample are prone to disturbances due to differences in the closure temperature of multiple phases. Particularly in the slowly cooled type 6 ordinary chondrites, the closure of individual minerals during different stages of the cooling history can result in a scatter of individual data point around the isochron because some phases may stay open while some of the others have already closed.

Two-point isochrons, however, are constructed from chromite and a fraction of the same sample that constitutes all of the remaining material. The two fractions represent two reservoirs where internal dis-equilibrium in one reservoir (silicates, metal), due to difference in the closure temperature of different phases will not affect the isochron. However, the isochron would be (partially) reset if chromite and the silicate fraction reservoir re-equilibrated during cooling. The type 3 samples investigated in the present study display a good agreement between the two-point isochron and chromite model ages (Fig. 8). In case of type 6 chondrites, the ages calculated by both methods agree within analytical uncertainties in samples SaU 228 (H6) and JaH 578 (H6) but show a mismatch in samples AHu 017 (L6) and Dho 1012 (L6). Apart from the re-equilibration between chromites and silicate fractions during cooling, impact disruption could be another reason for a disturbed isochron in samples AHu 017 (L6) and Dho 1012 (L6) leading to a mismatch between model ages and isochron ages in these two samples.

The Hf-W chronology data of ordinary chondrites indicate the possibility of impact disruptions of the ordinary chondrite parent bodies at ~10 Ma after CAI formation (Hellmann et al., 2019). According to the study, impacts of sufficient size and energy excavated material from the deep interior of the parent bodies of H, L and LL chon-

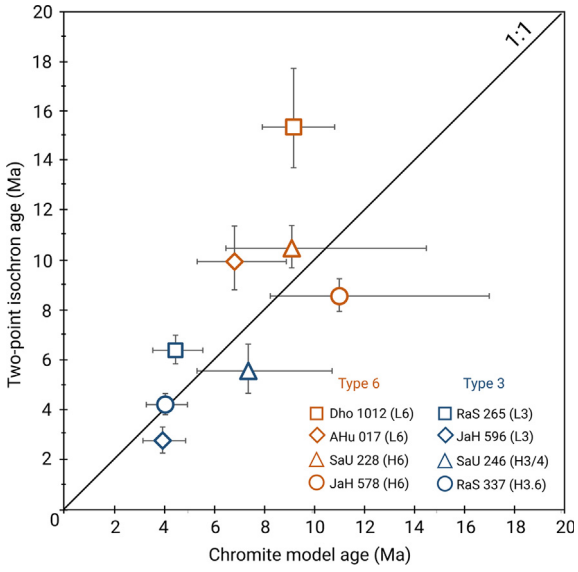

Fig. 8. A comparison between chromite model ages and two-point isochron ages determined for the studied samples. Type 3 samples show a good correlation in the two-point isochron and chromite model ages. The discrepancy between the two-point isochron and chromite model ages in the type 6 sample, AHu 017 (L6) and Dho 1012 (L6) is interpreted to be the result of their probable origin from an impact disturbed region on the parent bodies or partial re-equilibration during cooling from high temperatures.

drites, which is apparently the source of type 6 chondrite samples. Since only a few type 6 samples recorded disturbances in cooling history, an impact most likely disturbed only a limited part of the parent bodies of the ordinary chondrites. Any manifestation of the impact disrupted cooling histories in the Hf-W ages would also be recorded in Mn-Cr ages since the Hf-W ages record the cooling history at a closure temperature (~875 °C) higher than the Mn-Cr system (~760 °C).

The comparative study of two-point isochron and chromite model ages shows that two-point isochrons correlate well with the model ages in type 3 samples, but they remain prone to the impact-related disturbances or partial re-equilibration during cooling from high temperatures in type 6 samples. The results also demonstrate that the model ages derived from chromite constrain the time of mineral formation.

4.5. Time of accretion and cooling history for chondrite parent bodies

The earliest accretion of the ordinary chondrite parent bodies is constrained by the onset of chondrule formation. Hf-W data for ordinary chondrites show that metal-silicate fractionation among H, L and LL chondrites occurred between ~2 and ~2.7 Ma after CAIs which was coeval with the chondrule formation interval and prior to the accretion of chondrite parent bodies (Hellmann et al. 2019). Common isotope systems applied to determine chondrule ages are the long-lived, absolute ^{207}Pb-^{206}Pb (e.g., Bollard et al., 2017, 2019; Connelly et al., 2017; and references therein) and the short-lived ^{26}Al-^{26}Mg (e.g., Kita et al., 2000; Rudraswami and Goswami, 2007; Villeneuve et al., 2009; Kita and Ushikubo, 2012, Pape et al., 2019, Siron et al., 2020) chronometers. The ^{26}Al-^{26}Mg chronometer relies on the assumption of initial homogeneous distribution of the parent radionuclide throughout the inner protoplanetary disk. Pape et al. (2019) presented ^{26}Al-^{26}Mg ages for the formation of melt in individual chondrules from a wide range of chondrule types and mesostasis compositions and determined ages between $1.76^{+0.36}_{-0.27}$ Ma and $2.92^{+0.51}_{-0.34}$ Ma after CAI formation with a peak in chondrule formation at 2.0 and 2.3 Ma. A narrower interval of chondrule formation from ~1.80 to ~2.16 Ma after CAIs has been reported by Siron et al. (2020), however, the investigated chondrules are limited to anorthite-bearing chondrule type. Siron et al. (2020) noted that the youngest formation ages for anorthite-bearing chondrules are similar to the time of accretion for the ordinary chondrite parent bodies at ~2.1 Ma after CAIs, suggested in thermal evolution modelling studies (Sugiura and Fujiya, 2014; Blackburn et al., 2017). The two youngest chondrules from unequilibrated ordinary chondrites reported by Pape et al. (2019) record an age of ~2.92 Ma, of which one sample has been interpreted to date the time of partial remelting after primary formation in the protoplanetary disk (Pape et al., 2021). The melting and remelting events must have occurred before incorporation of chondrules into the chondrite parent body since the investigated samples are of low petrographic type and did not exceed temperatures in excess of ~300 °C after accretion. Moreover, since the ages are mostly defined by the Al-Mg systematics of pristine glass, they are interpreted to record the time of chondrule formation rather than a later thermal overprint. If main accretion of the chondrite parent bodies started at or shortly after ~2.1 Ma, it must have continued until ~3 Ma after CAI in order to account for the large number of chondrules recording younger melting and remelting ages.

Type 3 sample JaH 596 (L3) investigated in the present study records the oldest chromite model age of $3.99^{+0.93}_{-0.79}$ and a two-point isochron age of $2.78^{+0.55}_{-0.50}$ Ma after CAI formation. Neither the isochron nor the chromite model ages directly relate to the process of accretion. They date the formation of new mineral phases on their parent body which requires a thermal overprint after completion of accretion. Since type 3 chondrites represent the last accreted material on the chondrite parent bodies, the type 3 chromite model/isochron ages provide a limit for the latest time of accretion. Combined with the ^{26}Al-^{26}Mg chondrule formation ages, the final accretion of the ordinary chondrite parent bodies can be constrained after ~2.1 Ma but before ~3.4 Ma.

Whether the accretion of the chondrite parent bodies was instantaneous (~0.1 Myr) or protracted (≥1 Myr) has been a subject of a number of studies (e.g., Ghosh et al., 2003; Sahijpal et al., 2007; Neumann et al., 2012, Henke et al., 2013). Theoretical models for planetesimal formation and growth imply that the main period of acquisition of matter by large bodies in a planetesimal swarm was as short as 0.1 Ma (e.g., Nagasawa et al., 2007; Weidenschilling and

Cuzzi, 2006; Weidenschilling, 2011). In a recent study, Roth et al. (2016) investigated the cosmic-ray exposure ages of chondrules from L and LL ordinary chondrites and reported absence of detectable pre compaction exposure, suggesting rapid accretion (and/or efficient shielding from galactic cosmic ray and solar cosmic ray in the solar nebula). Chondrules from CR chondrites are reported to show some late irradiation effects consistent with the later accretion of their parent body as compared to the parent bodies of other chondrites (Beyersdorf-Kuis et al. 2015). An incremental or protracted accretion of the chondrite parent bodies would likely result in chemical fractionation that would appear as chemical differences between early accreting type 6 and late accreting type 3 chondrites. The lack of systematic chemical and nucleosynthetic isotopic variations between type 3 and type 6 meteorites implies that the accretion was rather instantaneous and not protracted.

Post accretion, type 3 material being farthest away from the centre of the parent bodies would have to reach peak metamorphic temperature of ~600 °C necessary to alter or produce chromites investigated in the present study. The nearly ubiquitous signs of thermal alteration of ordinary chondrites indicate that such temperatures were attained soon after accretion (Weidenschilling, 2019).

The processes leading to the accretion of parent bodies are highly debated (e.g., Weidenschilling, 2019). The key challenge is to reconcile the early formation of the differentiated parent bodies of the oldest iron meteorites with the delayed accretion of the chondrite parent bodies. ^{207}Pb-^{206}Pb and Hf-W dating of most achondrites suggest that their parent body differentiation predates the formation of chondrules and the accretion of the chondrite parent bodies (Baker et al., 2005; Bizzarro et al., 2005, Kleine et al., 2005). The radioactive decay of short-lived ^{26}Al ($t_{1/2}$ ~ 0.73 Ma) is considered to be the primary source of energy for asteroidal melting (e.g., Bizzarro et al., 2005). Since chondrites escaped melting but were heated enough to experience thermal metamorphism, it is generally assumed that they began accreting when a substantial fraction of ^{26}Al had decayed before the accretion was complete (e.g., Hevey and Sanders, 2006; Weidenschilling, 2019). Rubin (2010, 2011) proposed that in accordance with the petrographic properties, chemical and isotopic compositions, and volatile contents, different chondrite groups formed in regions at increasing heliocentric distance in the order of EH-El, OC, R, CR, CV-CK, CM-CO and CI. Based on Mn-Cr ages of secondary carbonates, the accretion ages are proposed to be at ~3.5 Ma for CM (Fujiya et al., 2012) and up to 3.9 Ma (Fujiya et al., 2013) for CI parent bodies (de Leuw et al., 2009; Visser et al., 2020). Jogo et al. (2017) studied the chemical compositions of CV3 fayalite and its Mn-Cr isotope systematics and proposed that the CV parent body accreted at about 3.2–3.3 Ma after CAI formation and is slightly younger than the ordinary chondrites parent bodies. Younger accretion ages (>3 Ma after CAIs) of the parent bodies of carbonaceous chondrites compared to ordinary chondrite parent bodies suggest an even lower fraction of short-lived ^{26}Al, as the primary source of energy at the time of their accretion. This is evident in the low thermal metamorphism recorded in carbonaceous chondrites. However, both carbonaceous and ordinary chondrites yield coeval (L and LL OCs and CO and CV meteorites, Pape et al., 2019) chondrule formation intervals. This suggests that the accretion of CC parent bodies was protracted and contemporary with the later stages of the chondrule formation event(s). Such a scenario buttresses the models that suggest a causal relationship between chondrule production and chondrite parent bodies accretion (Budde et al., 2016; Alexander et al., 2008; Edwards and Blackburn, 2020).

Metamorphism of the H and L chondrite parent bodies following the accretion of the planetesimals can be evaluated employing thermal evolution models that are constructed using increasingly complex physical input parameters (e.g., Trieloff et al., 2003; Hevey and Sanders, 2006; Sahijpal et al., 2007; Sahijpal and Gupta, 2011; Kleine et al., 2008; Harrison and Grimm, 2010; Henke et al., 2012a,b, 2013; Gail et al., 2015; Gail and Trieloff, 2018). To ensure model optimization, those meteorites are generally selected for which three or more cooling ages, reflecting different steps in the thermal history of the parent bodies (i.e., closure temperatures), are available. This constrains the slope as well as the curvature of individual cooling paths at their depths within the parent bodies. Although the chondrite samples investigated in the present study have not been dated with other chronometers, their determined chromite model ages and estimated closure temperatures can be used to test the validity of existing thermal models.

For the H and L chondrite parent bodies, thermal models show that the observed properties of chondrites are consistent with an "onion shell" model and a radius of about 100 km (Benoit et al., 2002; Trieloff et al., 2003; Hevey and Sanders, 2006; Bouvier et al., 2007; Sahijpal et al., 2007; Sahijpal and Gupta, 2011; Kleine et al., 2008; Harrison and Grimm, 2010; Henke et al., 2012a,b, 2013; Mare et al., 2014; Gail et al., 2015; Blackburn et al., 2017; Gail and Trieloff, 2018, Gail and Trieloff, 2019). The "onion shell" model predicts that higher temperatures are achieved at greater depths and slightly different times during the evolution of the chondrites parent bodies (e.g., Pellas, 1981; Trieloff et al., 2003). The chondrite samples investigated here display similar ranges in both two-point isochron and chromite model ages and the absolute ages correlate with the petrological grade for both H and L chondrites (Fig. 8) indicating similar structures, sizes, accretion time and high-temperature cooling histories for the parent bodies of both H and L classes. A narrow range in the chromite model ages for type 3 samples from $3.99^{+0.93}_{-0.79}$ to $4.51^{+1.10}_{-0.91}$ Ma suggests that the unmetamorphosed material surrounding the metamorphic core corresponds to a significantly narrower depth-range than the high-grade material i.e., type 6 samples that show wider timespan of chromite model ages from $6.9^{+2.1}_{-1.5}$ to$11.1^{+6.0}_{-2.8}$ Ma. The difference in the mean chromite model ages from type 3 and 6 samples is ~5 Myr which agrees with the difference of ~5.5 Myr as determined by Hf-W (Hellmann et al., 2019), but is much shorter than the interval of ~50 Myr derived from ^{207}Pb-^{206}Pb phosphate ages (Blackburn et al., 2017). The shorter intervals defined by the Mn-Cr and Hf-W sys-

tems date the earliest evolution processes of chondrite parent bodies and play a critical role in determining the time peak temperatures were reached in thermal evolution models.

Most thermal history models for both H and L chondrites assume that the parent bodies accreted at ~2 Ma after CAI formation, were heated dominantly by the decay of short-lived radioactive nuclides (^{26}Al and ^{60}Fe) and then cooled down after having reached the thermal peak over a period of ~100 Ma (e.g., Henke et al., 2012a,b, 2013; Gail et al., 2015; Gail and Trieloff, 2018). The Mn-Cr chromite model ages (Fig. 4, Table 5) and the inferred time of accretion of the ordinary chondrite parent bodies suggested in the present study are consistent with a thermal evolution where the accretion of the parent body began at or shortly after 2.1 Ma (post CAI formation). The center of the parent body reached the peak temperature at ~9 Ma after CAI formation, consistent with the mean chromite model age (9.1 ± 1.5 Ma, 2SE, $n = 4$) and closure temperature estimate (~760 °C) for type 6 chondrites. At shallower depths, the parent body reached a peak temperature of ~600 °C at ~4 Ma after CAI formation consistent with the mean of the two-point isochron and chromite model ages of 4.2 ± 1.0 Ma (2SE, $n = 6$) obtained for the investigated type 3 chondrites.

5. CONCLUSIONS

The Mn-Cr chromite model ages obtained in the present study range from $3.99^{+0.93}_{-0.79}$ Ma to $4.51^{+1.10}_{-0.91}$ Ma for type 3 and $6.9^{+2.1}_{-1.5}$ Ma to$11.1^{+6.0}_{-2.8}$ Ma for type 6, H and L ordinary chondrites. Chromite-silicate isochrons for the same samples range from $2.78^{+0.55}_{-0.50}$ to $15.4^{+2.4}_{-1.6}$ Ma. Both chromite model ages and isochron ages support an onion-shell structure of their parent bodies. Together with the closure temperature estimates for the Mn-Cr system in spinel, the model ages are inferred to constraint the peak metamorphic conditions for the unequilibrated type 3 chondrites and a time of Mn-Cr closure during retrograde metamorphism in type 6 chondrites. The model ages are consistent with a homogenous distribution of ^{53}Mn, a canonical ^{53}Mn/^{55}Mn $= 6.28 \times 10^{-6}$ and are in good agreement with the Hf-W ages for type 4, 5 and 6 ordinary chondrites (Hellmann et al., 2019). The high closure temperature estimates for Mn-Cr (~760 °C) and Hf-W (~870 °C) systems imply that the corresponding chronometers provide constraints on the peak-temperature metamorphic history of the ordinary chondrite parent bodies. This information is not obtainable from other chronometers such as ^{207}Pb-^{206}Pb due to their lower closure temperatures. The two-point isochron ages obtained for the chondrites agree within uncertainties with the respective chromite model ages except in samples JaH 578 (H6) and Dho 1012 (L6), where an impact-related disturbance during cooling from high temperatures could be the reason for partial re-equilibration of the Mn-Cr system. The results obtained in the present study indicate that the chromite model age approach is robust and yields age constraints that agree with those derived from chromite-silicate isochrons. This model-age approach for dating can also be extended to other meteoritic classes with chondritic Mn/Cr ratios. The oldest chromite model ages from type 3 samples, together with the Al-Mg chondrules formation ages (Kita et al., 2000; Rudraswami and Goswami, 2007; Villeneuve et al., 2009; Kita and Ushikubo, 2012; Pape et al., 2019; Siron et al., 2020), constrain the time of accretion of the ordinary chondrite parent bodies to >2.1 Ma after CAI formation. This age is in agreement with the previously estimated time of accretion for the ordinary chondrite parent bodies (Miyamoto et al., 1982; Göpel et al., 1994; Harrison and Grimm, 2010; Sugiura and Fujiya 2014; Doyle et al., 2015). The Mn-Cr chromite model ages and ^{26}Al-^{26}Mg chondrule formation ages are consistent with a thermal evolution model in which the accretion of the ordinary chondrite parent bodies began at or shortly after 2.1 Ma (post CAI formation) and the centre of the H chondrite parent body reached the peak temperature at ~9 Ma followed by cooling. The ordinary chondrite parent bodies accreted ~1 Ma later than the parent bodies of magmatic iron meteorites (Kleine et al., 2005; Scherstén et al., 2006; Burkhardt et al., 2008; Qin et al., 2008) and differentiated asteroids (e.g., acapulcoite-lodranite parent body, Touboul et al., 2009) but prior to the accretion of the carbonaceous chondrite parent bodies providing a coherent timeline of the meteorite parent bodies accretion. The coeval chondrule formation interval in carbonaceous and ordinary chondrites but younger (>3 Ma after CAIs) accretion ages suggest that accretion of the parent bodies of carbonaceous chondrites was protracted and contemporary to the later stages of chondrules formation event. This implies that there could be a causal relationship between chondrule formation and subsequent planetesimal accretion (Budde et al., 2016; Alexander et al., 2008; Edwards and Blackburn, 2020).

Declaration of Competing Interest

The authors declare that they have no known competing financial interests or personal relationships that could have appeared to influence the work reported in this paper.

ACKNOWLEDGEMENTS

This study was partially funded by 'Swiss Government Excellence Scholarship (2018.0371)'. We acknowledge funding within the framework of the NCCR PlanetS supported by the Swiss National Science Foundation grant nr. 51NF40-141881. We are grateful to B. Hofmann from the Natural History Museum Bern for providing all the ordinary chondrites samples investigated in this study. We acknowledge Patrick Neuhaus from the Institute of Geography, University of Bern for technical help and assistance with the ICP-MS analysis of the samples. We also thank Y. Kadlag and J. Hoffmann for their support and helpful discussions throughout the study. We thank Noriko Kita for editorial handling and Devin Schrader and two anonymous reviewers for their constructive comments that helped to improve the paper.

APPENDIX A. SUPPLEMENTARY MATERIAL

Supplementary data to this article can be found online at https://doi.org/10.1016/j.gca.2021.04.029.

REFERENCES

Alexander C. M. O'D., Grossman J. N., Ebel D. S. and Ciesla F. J. (2008) The formation conditions of chondrules and chondrites. *Science* **320**, 1617–1619.

Amelin Y., Kaltenbach A., Iizuka T., Stirling C. H., Ireland T. R., Petaev M. and Jacobsen S. B. (2010) U-Pb chronology of the Solar System's oldest solids with variable $^{238}U/^{235}U$. *Earth Planet. Sci. Lett.* **300**(3–4), 343–350.

Armstrong J. T. (1995) CITZAF: A package of correction programs for the quantitative electron microbeam X-ray-analysis of thick polished materials, thin films, and particles. *Microbeam Anal.* **4**, 177–200.

Baker J., Bizzarro M., Wittig N., Connelly J. and Haack H. (2005) Early planetesimal melting from an age of 4.5662 Gyr for differentiated meteorites. *Nature* **436**, 1127–1131.

Benedix G. K., Lauretta D. S. and McCoy T. J. (2005) Thermodynamic constraints on the formation conditions of winonaites and silicate-bearing IAB irons. *Geochim. Cosmochim. Acta* **69**, 5123–5131.

Benoit P. H., Akridge G. A., Ninagawa K. and Sears D. W. G. (2002) Thermoluminescence sensitivity and thermal history of type 3 ordinary chondrites: Eleven new type 3.0-3.1 chondrites and possible explanations for differences among H, L, and LL chondrites. *Meteorit. Planet. Sci.* **37**, 793–805.

Beyersdorf-Kuis U., Ott U. and Trieloff M. (2015) Early cosmic ray irradiation of chondrules and prolonged accretion of primitive meteorites. *Earth Planet. Sci. Lett.* **423**, 13–23.

Birck J. L. and Allègre C. J. (1985a) Evidence for the presence of ^{53}Mn in the early solar system. *Geophys. Res. Lett.* **12**, 745–748.

Birck J. L. and Allègre C. J. (1985b) Isotopes produced by galactic cosmic rays in iron meteorites. *Isotopic Ratios Sol. Syst.* **1**, 21–25.

Birck J. L. and Allègre C. J. (1988) Manganese-chromium isotope systematics and the development of the early Solar System. *Nature* **331**, 579–584.

Birck J. L., Rotaru M. and Allègre C. J. (1999) ^{53}Mn-^{53}Cr evolution of the early solar system. *Geochim. Cosmochim. Acta* **63**, 4111–4117.

Bizzarro M., Baker J. A., Haack H. and Lundgaard K. L. (2005) Rapid timescales for accretion and melting of differentiated planetesimals inferred from ^{26}Al-^{26}Mg chronometry. *Astrophys. J.* **632**, L41–L44.

Blackburn T., Alexander C. M. O'D., Carlson R. and Elkins-Tanton L. T. (2017) The accretion and impact history of the ordinary chondrite parent bodies. *Geochim. Cosmochim. Acta* **200**, 201–217.

Bollard J., Connelly J. N., Whitehouse M. J., Pringle E. A., Bonal L., Jørgensen J. K., Nordlund Å., Moynier F. and Bizzarro M. (2017) Early formation of planetary building blocks inferred from Pb isotopic ages of chondrules. *Sci. Adv.* **3** e1700407.

Bollard J., Kawasaki N., Sakamoto N., Olsen M., Itoh S., Larsen K., Wielandt D., Schiller M., Connelly J. N., Yurimoto H. and Bizzarro M. (2019) Combined U-corrected Pb-Pb dating and ^{26}Al-^{26}Mg systematics of individual chondrules–Evidence for a reduced initial abundance of ^{26}Al amongst inner Solar System chondrules. *Geochim. Cosmochim. Acta* **260**, 62–83.

Bouvier A., Blichert-Toft J., Moynier F., Vervoort J. D. and Albarède F. (2007) Pb-Pb dating constraints on the accretion and cooling history of chondrites. *Geochim. Cosmochim. Acta* **71**, 1583–1604.

Budde G., Kleine T., Kruijer T. S., Burkhardt C. and Metzler K. (2016) Tungsten isotopic constraints on the age and origin of chondrules. *Proc. Natl. Acad. Sci. U. S. A.* **113**, 2886–2891.

Bunch T., Keil K. and Snetsinger K. G. (1967) Chromite composition in relation to chemistry and texture of ordinary chondrites. *Geochim. Cosmochim. Acta* **31**, 1569–1582.

Burkhardt C., Kleine T., Bourdon B., Palme H., Zipfel J., Friedrich J. M. and Ebel D. S. (2008) Hf-W mineral isochron for Ca, Al-rich inclusions: Age of the solar system and the timing of core formation in planetesimals. *Geochim. Cosmochim. Acta* **72**, 6177–6197.

Busemann H., Alexander M. O. D. and Nittler L. R. (2007) Characterization of insoluble organic matter in primitive meteorites by microRaman spectroscopy. *Meteorit. Planet. Sci.* **42**, 1387–1416.

Cherniak D. J., Lanford W. A. and Ryerson F. J. (1991) Lead diffusion in apatite and zircon using ion implantation and Rutherford Backscattering techniques. *Geochim. Cosmochim. Acta* **55**, 1663–1673.

Connelly J. N., Bollard J. and Bizzarro M. (2017) Pb-Pb chronometry and the early Solar System. *Geochim. Cosmochim. Acta* **201**, 345–363.

DeHart J. M., Lofgren G. E., Jie L., Benoit P. H. and Sears D. W. G. (1992) Chemical and physical studies of chondrites: X. Cathodoluminescence and phase composition studies of metamorphism and nebular processes in chondrules of type 3 ordinary chondrites. *Geochim. Cosmochim. Acta* **56**, 3791–3807.

de Leuw S., Rubin A. E., Schmitt A. K. and Wasson J. T. (2009) ^{53}Mn-^{53}Cr systematics of carbonates in CM chondrites: implications for the timing and duration of aqueous alteration. *Geochim Cosmochim. Act* **73**, 7433–7442.

Dodd, R.T., 1981. Meteorites-A Petrologic-Chemical Synthesis, Cambridge, p. 368.

Dodson M. H. (1973) Closure temperature in cooling geochronological and petrological systems. *Contrib. Mineral. Petrol.* **40**, 259–274.

Doyle P. M., Jogo K., Nagashima K., Krot A. N., Wakita S., Ciesla F. J. and Hutcheon I. D. (2015) Early aqueous activity on the ordinary and carbonaceous chondrite parent bodies recorded by fayalite. *Nat. Commun.* **6**, 1–10.

Edwards G. H. and Blackburn T. (2020) Accretion of a large LL parent planetesimal from a recently formed chondrule population. *Sci. Adv.* **6**, 1–9.

Ferracutti G. R., Gargiulo M. F., Ganuza M. L., Bjerg E. A. and Castro S. M. (2015) Determination of the spinel group end-members based on electron microprobe analyses. *Mineral. Petrol.* **109**, 153–160.

Fujiya W., Sugiura N., Hotta H., Ichimura K. and Sano Y. (2012) Evidence for the late formation of hydrous asteroids from young meteoritic carbonates. *Nat. Commun.* **3**, 1–6.

Fujiya W., Sugiura N., Sano Y. and Hiyagon H. (2013) Mn-Cr ages of dolomites in CI chondrites and the Tagish Lake ungrouped carbonaceous chondrite. *Earth Planet. Sci. Lett.* **362**, 130–142.

Gail H. P., Henke S. and Trieloff M. (2015) Thermal evolution and sintering of chondritic planetesimals: II. Improved treatment of the compaction process. *Astron. Astrophys.* **576**.

Gail H. P. and Trieloff M. (2018) Thermal evolution and sintering of chondritic planetesimals IV. Temperature dependence of heat conductivity of asteroids and meteorites. *Astron. Astrophys.* **615**.

Gail H. P. and Trieloff M. (2019) Thermal history modelling of the L chondrite parent body. *Astron. Astrophys.* **628**, A77.

Ganguly J., Ito M. and Zhang X. (2007) Cr diffusion in orthopyroxene: Experimental determination, ^{53}Mn-^{53}Cr thermochronology, and planetary applications. *Geochim. Cosmochim. Acta* **71**, 3915–3925.

Ganguly, J., Tirone, M., 2009. Closure Temperature, Cooling Age and High Temperature Thermochronology. Phys. Chem. Earth's Inter., Springer, New York, NY, pp. 89–99.
Ganguly J., Tirone M., Chakraborty S. and Domanik K. (2013) H-chondrite parent asteroid: A multistage cooling, fragmentation and re-accretion history constrained by thermometric studies, diffusion kinetic modeling and geochronological data. *Geochim. Cosmochim. Acta* **105**, 206–220.
Ganguly J., Tirone M. and Domanik K. (2016) Cooling rates of LL, L and H chondrites and constraints on the duration of peak thermal conditions: Diffusion kinetic modeling and implications for fragmentation of asteroids and impact resetting of petrologic types. *Geochim. Cosmochim. Acta* **192**, 135–148.
Ghosh A., Weidenschilling S. J. and McSween H. Y. (2003) Importance of the accretion process in asteroid thermal evolution: 6 Hebe as an example. *Meteorit. Planet. Sci.* **38**, 711–724.
Göpel C., Manhès G. and Allègre C. J. (1994) U-Pb systematics of phosphates from equilibrated ordinary chondrites. *Earth Planet. Sci. Lett.* **121**, 153–171.
Göpel C., Birck J. L., Galy A., Barrat J. A. and Zanda B. (2015) Mn-Cr systematics in primitive meteorites: Insights from mineral separation and partial dissolution. *Geochim. Cosmochim. Acta* **156**, 1–24.
Grossman J. N. and Brearley A. J. (2005) The onset of metamorphism in ordinary and carbonaceous chondrites. *Meteorit. Planet. Sci.* **40**, 87–122.
Harrison K. P. and Grimm R. E. (2010) Thermal constraints on the early history of the H-chondrite parent body reconsidered. *Geochim. Cosmochim. Acta* **74**, 5410–5423.
Hellmann J. L., Kruijer T. S., Van Orman J. A., Metzler K. and Kleine T. (2019) Hf-W chronology of ordinary chondrites. *Geochim. Cosmochim. Acta* **258**, 290–309.
Henke S., Gail H. P., Trieloff M., Schwarz W. H. and Kleine T. (2012a) Thermal evolution and sintering of chondritic planetesimals. *Astron. Astrophys.* **537**.
Henke S., Gail H. P., Trieloff M., Schwarz W. H. and Kleine T. (2012b) Thermal history modelling of the H chondrite parent body. *Astron. Astrophys.* **545**.
Henke S., Gail H. P., Trieloff M. and Schwarz W. H. (2013) Thermal evolution model for the H chondrite asteroid-instantaneous formation versus protracted accretion. *Icarus* **226**, 212–228.
Hevey P. J. and Sanders I. S. (2006) A model for planetesimal meltdown by ^{26}Al and its implications for meteorite parent bodies. *Meteorit. Planet. Sci.* **41**, 95–106.
Honda M. and Imamura M. (1971) Half-life of ^{53}Mn. *Phys. Rev. C* **4**, 1182–1188.
Huss G. R., Rubin A. E. and Grossman J. N. (2006) Thermal Metamorphism in Chondrites. *Meteorites Early Sol. Syst.* **II**, 567–586.
Ito M. and Ganguly J. (2006) Diffusion kinetics of Cr in olivine and ^{53}Mn-^{53}Cr thermochronology of early solar system objects. *Geochim. Cosmochim. Acta* **70**, 799–809.
Jacobsen B., Yin Q.-Z., Moynier F., Amelin Y., Krot A. N., Nagashima K., Hutcheon I. D. and Palme H. (2008) ^{26}Al-^{26}Mg and ^{207}Pb-^{206}Pb systematics of Allende CAIs: Canonical solar initial ^{26}Al/^{27}Al ratio reinstated. *Earth Planet. Sci. Lett.* **272**, 353–364.
Jogo K., Nakamura T., Ito M., Wakita S., Zolotov M. Y. and Messenger S. R. (2017) Mn-Cr ages and formation conditions of fayalite in CV3 carbonaceous chondrites: Constraints on the accretion ages of chondritic asteroids. *Geochim. Cosmochim. Acta* **199**, 58–74.
Johnson C. A. and Prinz M. (1991) Chromite and olivine in type II chondrules in carbonaceous and ordinary chondrites: Implications for thermal histories and group differences. *Geochim. Cosmochim. Acta* **55**, 893–904.
Keil K., Lange D., Ulbrich M. N. C., Gomes C. B., Jarosewich E., Roisenberg A. and Souza M. J. (1978a) Studies of Brazilian meteorites XIII. Mineralogy, petrology, and chemistry of the Putinga, Rio Grande do Sul, chondrite. *Meteoritics* **13**, 165–175.
Keil K., Lux G., Brookins D. G., King E. A., King T. V. V. and Jarosewich E. (1978b) The Inman, McPherson County, Kansas meteorite. *Meteoritics* **13**, 11–22.
Kessel R., Beckett J. R. and Stolper E. M. (2007) The thermal history of equilibrated ordinary chondrites and the relationship between textural maturity and temperature. *Geochim. Cosmochim. Acta* **71**, 1855–1881.
Kimura M., Nakajima H., Hiyagon H. and Weisberg M. K. (2006) Spinel group minerals in LL3.00-6 chondrites: Indicators of nebular and parent body processes. *Geochim. Cosmochim. Acta* **70**, 5634–5650.
Kita N. T., Nagahara H., Togashi S. and Morishita Y. (2000) A short duration of chondrule formation in the solar nebula: Evidence from ^{26}Al in Semarkona ferromagnesian chondrules. *Geochim. Cosmochim. Acta* **64**, 3913–3922.
Kita N. T. and Ushikubo T. (2012) Evolution of protoplanetary disk inferred from 26Al chronology of individual chondrules. *Meteorit. Planet. Sci.* **47**, 1108–1119.
Kleine T., Hans U., Irving A. J. and Bourdon B. (2012) Chronology of the angrite parent body and implications for core formation in protoplanets. *Geochim. Cosmochim. Acta* **84**, 186–203.
Kleine T., Mezger K., Palme H., Scherer E. and Münker C. (2005) Early core formation in asteroids and late accretion of chondrite parent bodies: Evidence from ^{182}Hf-^{182}W in CAIs, metal-rich chondrites, and iron meteorites. *Geochim. Cosmochim. Acta* **69**, 5805–5818.
Kleine T., Touboul M., Van Orman J. A., Bourdon B., Maden C., Mezger K. and Halliday A. N. (2008) Hf-W thermochronometry: Closure temperature and constraints on the accretion and cooling history of the H chondrite parent body. *Earth Planet. Sci. Lett.* **270**, 106–118.
Larsen K. K., Trinquier A., Paton C., Schiller M., Wielandt D., Ivanova M. A., Connelly J. N., Nordlund A., Krot A. N. and Bizzarro M. (2011) Evidence for magnesium isotope hetero- geneity in the solar protoplanetary disk. *Astrophys. J. Lett.* **735**, L37–L44.
Lindsley D. H. and Andersen D. J. (1983) A two-pyroxene thermometer. *J. Geophys. Res.* **88**, A887–A906.
Liu J., Qin L., Xia J., Carlson R. W., Leya I., Dauphas N. and He Y. (2019) Cosmogenic effects on chromium isotopes in meteorites. *Geochim. Cosmochim. Acta* **251**, 73–86.
Lugmair G. W. and Shukolyukov A. (1998) Early solar system timescales according to ^{53}Mn-^{53}Cr systematics. *Geochim. Cosmochim. Acta* **62**, 2863–2886.
Mahan B., Moynier F., Siebert J., Gueguen B., Agranier A., Pringle E. A., Bollard J., Connelly J. N. and Bizzarro M. (2018) Volatile element evolution of chondrules through time. *Proc. Natl. Acad. Sci.* **115**, 8547–8552.
Mare E. R., Tomkins A. G. and Godel B. M. (2014) Restriction of parent body heating by metal-troilite melting: Thermal models for the ordinary chondrites. *Meteorit. Planet. Sci.* **49**, 636–651.
Matthes M., van Orman J. A. and Kleine T. (2020) Closure temperature of the Pd-Ag system and the crystallization and cooling history of IIIAB iron meteorites. *Geochim. Cosmochim. Acta* **285**, 193–206.
McCoy T. J., Scott E. R. D., Jones R. H., Keil K. and Taylor G. J. (1991) Composition of chondrule silicates in LL3-5 chondrites and implications for their nebular history and parent body metamorphism. *Geochim. Cosmochim. Acta* **55**, 601–619.

Miyamoto M., Fujii N. and Takeda H. (1982) Ordinary chondrite parent body-An internal heating model. *Lunar Planet. Sci. Conf. Proc.* **12**, 1145–1152.

Moynier F., Yin Q.-Z. and Jacobsen B. (2007) Dating the first stage of planet formation. *Astrophys. J.* **671**, L181–L183.

Nagasawa M., Thommes E. W., Kenyon S. J., Bromley B. C. and Lin D. N. C. (2007) Thediverse origins of terrestrial-planet systems. *Protostars Planets V*, 639–654.

Neumann W., Breuer D. and Spohn T. (2012) Differentiation and core formation in accreting planetesimals. *Astron. Astrophys.* **543**, A141.

Nyquist L. E., Kleine T., Shih C. Y. and Reese Y. D. (2009) The distribution of short-lived radioisotopes in the early solar system and the chronology of asteroid accretion, differentiation, and secondary mineralization. *Geochim. Cosmochim. Acta* **73**, 5115–5136.

Nyquist L., Lindstrom D., Mittlefehldt D., Shih C. Y., Wiesmann H., Wentworth S. and Martinez R. (2001) Manganese-chromium formation intervals for chondrules from the Bishunpur and Chainpur meteorites. *Meteorit. Planet. Sci.* **36**, 911–938.

Pape J., Mezger K., Bouvier A. S. and Baumgartner L. P. (2019) Time and duration of chondrule formation: Constraints from ^{26}Al-^{26}Mg ages of individual chondrules. *Geochim. Cosmochim. Acta* **244**, 416–436.

Pape J., Rosén Å. V., Mezger K. and Guillong M. (2021) Primary crystallization and partial remelting of chondrules in the protoplanetary disk: Petrographic, mineralogical and chemical constraints recorded in zoned type-I chondrules. *Geochim. Cosmochim. Acta* **292**, 499–517.

Pedersen S. G., Schiller M., Connelly J. N. and Bizzarro M. (2019) Testing accretion mechanisms of the H chondrite parent body utilizing nucleosynthetic anomalies. *Meteorit. Planet. Sci.* **54**, 1215–1227.

Pellas P. S. D. (1981) ^{244}Pu fission track thermometry and its application to stony meteorites. *Proc. R. Soc. Lond. A. Math. Phys. Sci.* **374**, 253–270.

Posner E. S., Ganguly J. and Hervig R. (2016) Diffusion kinetics of Cr in spinel: Experimental studies and implications for ^{53}Mn-^{53}Cr cosmochronology. *Geochim. Cosmochim. Acta* **175**, 20–35.

Qin L., Alexander C. M. O. D., Carlson R. W., Horan M. F. and Yokoyama T. (2010) Contributors to chromium isotope variation of meteorites. *Geochim. Cosmochim. Acta* **74**, 1122–1145.

Qin L., Dauphas N., Wadhwa M., Masarik J. and Janney P. E. (2008) Rapid accretion and differentiation of iron meteorite parent bodies inferred from ^{182}Hf-^{182}W chronometry and thermal modeling. *Earth Planet. Sci. Lett.* **273**, 94–104.

Roth A. S. G., Metzler K., Baumgartner L. P. and Leya I. (2016) Cosmic-ray exposure ages of chondrules. *Meteorit. Planet. Sci.* **51**, 1256–1267.

Rubin A. E. (2011) Origin of the differences in refractory-lithophile-element abundances among chondrite groups. *Icarus* **213**, 547–558.

Rubin A. E. (2010) Physical properties of chondrules in different chondrite groups: Implications for multiple melting events in dusty environments. *Geochim. Cosmochim. Acta* **74**, 4807–4828.

Rudraswami N. G. and Goswami J. N. (2007) 26Al in chondrules from unequilibrated L chondrites: Onset and duration of chondrule formation in the early solar system. *Earth Planet. Sci. Lett.* **257**, 231–244.

Ruzicka A., Snyder G. A. and Taylor L. A. (1998) Mega-chondrules and large, igneous-textured clasts in Julesberg (L3) and other ordinary chondrites: vapor-fractionation, shock-melting, and chondrule formation. *Geochim. Cosmochim. Acta* **62**, 1419–1442.

Sack R. O. and Ghiorso M. S. (1989) Importance of considerations of mixing properties in establishing an internally consistent thermodynamic database: thermochemistry of minerals in the system Mg_2SiO_4-Fe_2SiO_4-SiO_2. *Contrib. Mineral. Petrol.* **102**, 41–68.

Sack Richard O. and Ghiorso M. S. (1991a) An internally consistent model for the thermodynamic properties of Fe-Mg-titanomagnetite-aluminate spinels. *Contrib. Mineral. Petrol.* **106**, 474–505.

Sack R. O. and Ghiorso M. S. (1991b) Chromian spinels as petrogenetic indicators: thermodynamics and petrological applications. *Am. Mineral.* **76**, 827–847.

Sahijpal S. and Gupta G. (2011) Did the carbonaceous chondrites evolve in the crustal regions of partially differentiated asteroids?. *J. Geophys. Res.* **116**, E6.

Sahijpal S., Soni P. and Gupta G. (2007) Numerical simulations of the differentiation of accreting planetesimals with ^{26}Al and ^{60}Fe as the heat sources. *Meteorit. Planet. Sci.* **42**, 1529–1548.

Sanborn M. E., Wimpenny J., Williams C. D., Yamakawa A., Amelin Y., Irving A. J. and Yin Q.-Z. (2019) Carbonaceous achondrites Northwest Africa 6704/6693: milestones for early solar system chronology and genealogy. *Geochim. Cosmochim. Acta* **245**, 577–596.

Scherstén A., Elliott T., Hawkesworth C., Russell S. and Masarik J. (2006) Hf-W evidence for rapid differentiation of iron meteorite parent bodies. *Earth Planet. Sci. Lett.* **241**, 530–542.

Schneider J. M., Burkhardt C., Marrocchi Y., Brennecka G. A. and Kleine T. (2020) Early evolution of the solar accretion disk inferred from Cr-Ti-O isotopes in individual chondrules. *Earth Planet. Sci. Lett.* **551** 116585.

Schrader D. L., Davidson J. and McCoy T. J. (2016) Widespread evidence for high-temperature formation of pentlandite in chondrites. *Geochim. Cosmochim. Acta* **189**, 359–376.

Siron G., Fukuda K., Kimura M. and Kita N. T. (2020) New constraints from ^{26}Al-^{26}Mg chronology of anorthite bearing chondrules in unequilibrated ordinary chondrites. *Geochim. Cosmochim. Acta* **293**, 103–126.

Shukolyukov A. and Lugmair G. W. (2006) Manganese-chromium isotope systematics of carbonaceous chondrites. *Earth Planet. Sci. Lett.* **250**, 200–213.

Sievwright R. H., O'Neill H. S. C., Tolley J., Wilkinson J. J. and Berry A. J. (2020) Diffusion and partition coefficients of minor and trace elements in magnetite as a function of oxygen fugacity at 1150 °C. *Contrib. Mineral. Petrol.* **175**.

Slater-Reynolds V. and McSween H. Y. (2005) Peak metamorphic temperatures in type 6 ordinary chondrites: An evaluation of pyroxene and plagioclase geothermometry. *Meteorit. Planet. Sci.* **40**, 745–754.

Sugiura N. and Fujiya W. (2014) Correlated accretion ages and ε^{54}Cr of meteorite parent bodies and the evolution of the solar nebula. *Meteorit. Planet. Sci.* **49**, 772–787.

Sugiura N. and Hoshino H. (2003) Mn-Cr chronology of five IIIAB iron meteorites. *Meteorit. Planet. Sci.* **38**, 117–143.

Suzuki A. M., Yasuda A. and Ozawa K. (2008) Cr and Al diffusion in chromite spinel: Experimental determination and its implication for diffusion creep. *Phys. Chem. Miner.* **35**, 433–445.

Touboul M., Kleine T., Bourdon B., Van Orman J. A., Maden C. and Zipfel J. (2009) Hf-W thermochronometry: II. Accretion and thermal history of the acapulcoite-lodranite parent body. *Earth Planet. Sci. Lett.* **284**, 168–178.

Trieloff M., Jessberger E. K., Herrwerth I., Hopp J., Flénl C., Ghélis M., Bourot-Denise M. and Pellas P. (2003) Structure and thermal history of the H-chondrite parent asteroid revealed by thermochronometry. *Nature* **422**, 502–506.

Trinquier A., Birck J.-L. and Allègre C. J. (2007) Widespread ^{54}Cr heterogeneity in the inner solar system. *Astrophys. J.* **655**, 1179–1185.

Trinquier A., Birck J. L. and Allègre C. J. (2008a) High-precision analysis of chromium isotopes in terrestrial and meteorite samples by thermal ionization mass spectrometry. *J. Anal. At. Spectrom.* **23**, 1565–1574.

Trinquier A., Birck J. L., Allègre C. J., Göpel C. and Ulfbeck D. (2008b) ^{53}Mn-^{53}Cr systematics of the early Solar System revisited. *Geochim. Cosmochim. Acta* **72**, 5146–5163.

Van Schmus W. R. and Wood J. A. (1967) A chemical-petrologic classification for the chondritic meteorites. *Geochim. Cosmochim. Acta* **31**, 747–765.

Vermeesch P. (2018) IsoplotR: A free and open toolbox for geochronology. *Geosci. Front.* **9**, 1479–1493.

Villeneuve J., Chaussidon M. and Libourel G. (2009) Homogeneous distribution of ^{26}Al in the solar system from the Mg isotopic composition of chondrules. *Science* **325**, 985–988.

Visser R., John T., Whitehouse M. J., Patzek M. and Bischoff A. (2020) A short-lived ^{26}Al induced hydrothermal alteration event in the outer solar system: Constraints from Mn/Cr ages of carbonates. *Earth Planet. Sci. Lett.* **547** 116440.

Wasson J. T. and Allemeyn G. W. K. (1988) Compositions of chondrites. *Philos. Trans. R. Soc. Lond. Ser. A Math. Phys. Sci.* **325**, 535–544.

Weidenschilling S. J. (2019) Accretion of the asteroids: Implications for their thermal evolution. *Meteorit. Planet. Sci.* **54**, 1115–1132.

Weidenschilling S. J. (2011) Initial sizes of planetesimals and accretion of the asteroids. *Icarus* **214**, 671–684.

Weidenschilling S. J. and Cuzzi J. N. (2006) Accretion dynamics and timescales: Relation to chondrites. In *Meteorites and the Early Solar System* (eds. D. Lauretta and H. McSween). Univ. of Arizona Press, Tucson, pp. 473–485.

Wlotzka F. (1993) A weathering scale for the ordinary chondrites. *Meteoritics* **28**, 460.

Wlotzka F. (2005) Cr spinel and chromite as petrogenetic indicators in ordinary chondrites: Equilibration temperatures of petrologic types 3.7 to 6. *Meteorit. Planet. Sci.* **40**, 1673–1702.

Yanai K. and Kojima H. (1991) Yamato-74063: Chondritic meteorite classified between E and H chondrite groups. *Antarctic Meteorite Res.* **4**, 118.

Associate editor: Noriko T. Kita